DMD Fast Forward. Published on October 4, 2022 as DOI: 10.1124/dmd.122.000994
This article has not been copyedited and formatted. The final version may differ from this version.

Title Page

Assessing Liver-to-Plasma Partition Coefficients and In Silico Calculation Methods: When Does the Hepatic Model Matter in PBPK?

Xiaonan Li and William J. Jusko*

Department of Pharmaceutical Sciences, State University of New York at Buffalo, 404 Pharmacy Building, Buffalo, New York 14214, USA

Downloaded from dmd.aspetjournals.org at ASPET Journals on April 19, 2024

DMD Fast Forward. Published on October 4, 2022 as DOI: 10.1124/dmd.122.000994
This article has not been copyedited and formatted. The final version may differ from this version.

Running Title Page

Model-Dependent Hepatic Partition Coefficients

* **Corresponding author**

William J. Jusko, PhD

Department of Pharmaceutical Sciences, State University of New York at Buffalo, 404 Pharmacy Building, Buffalo, New York 14214, USA

E–mail: wjjusko@buffalo.edu

Number of text pages: 47

Number of tables: 4

Number of figures: 6

Number of references: 82

Number of words in Abstract: 249

Number of words in Introduction: 945

Number of words in Discussion: 1545

ABBREVIATIONS

AUC, area under the curve; CL_b, total blood clearance; $CL_{h:}$, hepatic clearance; CL_{int}, hepatic intrinsic clearance; CQ, chloroquine; CyA, cyclosporine A; DLZ, diltiazem; DM, dispersion model; DPH, phenytoin; DZP, diazepam; EB, ethoxybenzamide; ER, extraction ratio; FTY720, fingolimod; f_{ub}, unbound fraction in blood; f_{up}, unbound fraction in plasma; HB, hexobarbital; IP, intraperitoneal; IV, intravenous; IVIVE, *in vitro*-to-*in vivo* extrapolation; K_p, tissue-to-plasma partition coefficient; NIC, nicotine; PBPK, physiologically-based pharmacokinetic; PK, pharmacokinetic; PPN, propranolol; PTM, parallel tube model; PTZ, pentazocine; QD,

Downloaded from dmd.aspetjournals.org at ASPET Journals on April 19, 2024

DMD Fast Forward. Published on October 4, 2022 as DOI: 10.1124/dmd.122.000994
This article has not been copyedited and formatted. The final version may differ from this version.

quinidine; QSPR, quantitative structure-property relationships; R_b, blood-to-plasma ratio; SS, steady state; TB: tolbutamide; VEM, verapamil; WSM, well-stirred model.

Downloaded from dmd.aspetjournals.org at ASPET Journals on April 19, 2024

DMD Fast Forward. Published on October 4, 2022 as DOI: 10.1124/dmd.122.000994
This article has not been copyedited and formatted. The final version may differ from this version.

Abstract

The primary models used in pharmacokinetics (PK) to assess hepatic clearance (CL_h) are the well-stirred (WSM), parallel tube (PTM), and dispersion model (DM) that differ in their internal flow patterns and assumed unbound liver concentrations. Physiologically-Based Pharmacokinetic (PBPK) models require a hepatic intrinsic clearance (CL_{int}) and tissue-to-plasma partition coefficient (K_p). Given measured systemic and liver concentration-time profiles, these hepatic models perform similarly but yield model-specific CL_{int} and K_p estimates. This work provides mathematical relationships for the three basic hepatic models and assesses their corresponding PBPK-relevant K_p values with literature-reported single-dose blood and liver concentration-time data of 14 compounds. Model fittings were performed with an open-loop approach where the CL_h and extraction ratio (ER) were first estimated from fitting the blood data yielding CL_{int} values for the three hepatic models. The pre-fitted blood data served as forcing input functions to obtain PBPK-operative K_p estimates that were compared with those obtained by the tissue/plasma area ratio (AR), Chen & Gross (C&G) and published *in silico* methods. The CL_{int} and K_p values for the hepatic models increased with the ER and both showed a rank order being WSM > DM > PTM. Drugs with low ER showed no differences as expected. With model-specific CL_{int} and K_p values, all hepatic models predict the same steady-state K_p (K_p^{ss}) that is comparable to those from the AR and C&G methods and reported by direct measurement. All *in silico* methods performed poorly for most compounds. Hepatic model selection requires cautious application and interpretation in PBPK modeling.

Keywords Hepatic clearance models; Physiologically based pharmacokinetic modeling; Intrinsic clearance; Tissue-to-plasma partition coefficient

Downloaded from dmd.aspetjournals.org at ASPET Journals on April 19, 2024

DMD Fast Forward. Published on October 4, 2022 as DOI: 10.1124/dmd.122.000994
This article has not been copyedited and formatted. The final version may differ from this version.

Significance Statement

The three hepatic models generate different single-dose (non-steady-state) values of CL_{int} and K_p in PBPK models especially for drugs with high *ER*; however, all K_p^{ss} values expected from constant rate infusion studies were the same. These findings are relevant when using these models for *in vitro*-to-*in vivo* extrapolation (IVIVE) where a model-dependent CL_{int} is used to correct measured drug concentrations for depletion of the tissue by metabolism. This model-dependency may also have an impact when assessing the PK/pharmacodynamic relationships when effects relate to assumed hepatic concentrations.

Downloaded from dmd.aspetjournals.org at ASPET Journals on April 19, 2024

DMD Fast Forward. Published on October 4, 2022 as DOI: 10.1124/dmd.122.000994
This article has not been copyedited and formatted. The final version may differ from this version.

Introduction

Hepatic clearance (CL_h) was first extended from the concept of renal clearance by Lewis to describe elimination by the liver (Lewis, 1948). Later, it was further defined as the product of hepatic blood flow (Q_h) and extraction ratio (ER) (Rowland et al., 1973; Wilkinson and Shand, 1975), and has been one of the most critical parameters in pharmacokinetics (PK) and therapeutic development owing to the pivotal role of liver in eliminating numerous endogenous and exogenous compounds.

The primary models of hepatic elimination in PK to assess and predict the CL_h are the well-stirred (WSM), parallel tube (PTM), and dispersion model (DM) (Bass et al., 1976; Pang and Rowland, 1977; Roberts and Rowland, 1986a; Roberts and Rowland, 1986b). The shared assumptions of these basic hepatic clearance models are that only the unbound drug permeates the hepatocytes; drug distribution into liver is limited by the blood flow without any diffusion barriers; and there is equilibration between drug concentration in the liver and that in the emergent venous blood, i.e., the unbound drug concentration in blood relates to that in the tissue. While the major difference among these models lies in the assumed internal blood flow patterns that result in differing unbound drug concentrations along the sinusoidal flow path within the liver (e.g., bulk flow with infinite mixing creating uniform concentrations for the WSM, plug flow with no mixing resulting in a mono-exponential concentration decline for the PTM, and dispersive flow with some extent of mixing rendering a continuous concentration decline for the DM that lies in between those of the WSM and PTM). Although the WSM is the least physiological, the lesser complexities in math and easier operative feature have made it the most widely used hepatic model for making predictions of the *in vivo* CL_h using metabolic data obtained from various *in vitro* systems (*in vitro*-to-*in vivo* extrapolation, IVIVE) (Rane et al.,

Downloaded from dmd.aspetjournals.org at ASPET Journals on April 19, 2024

DMD Fast Forward. Published on October 4, 2022 as DOI: 10.1124/dmd.122.000994
This article has not been copyedited and formatted. The final version may differ from this version.

1977; Houston, 1994; Hallifax et al., 2010) and for applying physiologically-based pharmacokinetic (PBPK) models (Miller et al., 2019).

The WSM has been a vigorous topic of discussion in the PK field in describing the hepatic elimination process and predicting the *in vivo* CL_h by IVIVE (Roberts and Rowland, 1986a; Houston and Carlile, 1997; Iwatsubo et al., 1997; Naritomi et al., 2001; Ito and Houston, 2004; Kilford et al., 2009; Benet et al., 2018; Rowland and Pang, 2018; Pang et al., 2019; Sodhi et al., 2020). Nevertheless, the basic hepatic models remain highly useful as starting points in PK and PBPK in considerations of the hepatic distribution and elimination process for drugs. In practice, PBPK models of hepatic elimination require two important parameters when describing the hepatic disposition of a drug, i.e., the intrinsic clearance (CL_{int}) that reflects the innate ability of the liver to remove the drug from the body by metabolism or excretion with the reference concentration being the unbound drug within the organ and the liver-to-plasma partition coefficient (K_p) that represents the extent of drug distribution. Theoretically, given the same measured systemic and liver concentration-time profiles, these hepatic models yield model-specific CL_{int} and K_p estimates because of the differed intra-organ unbound concentrations. The theoretical expectations of the model dependencies in the CL_{int} and unbound tissue concentrations have been reviewed (Pang et al., 2019; Rowland et al., 2022). However, there have been no comprehensive comparisons of their applications in PBPK models and the resulting K_p values when assessing *in vivo* time course data. It also remains vague about how to incorporate the more realistic models of hepatic elimination (i.e., PTM and DM) in PBPK.

Values for K_p are needed in operation of PBPK models (as will be shown). The simplest concept of K_p originated with Gillette (Gillette, 1971) who considered it to be the ratio of the fraction of drug unbound in plasma (f_{up}) to fraction unbound in tissues (f_{uT}). Over time, the complexity of

Downloaded from dmd.aspetjournals.org at ASPET Journals on April 19, 2024

DMD Fast Forward. Published on October 4, 2022 as DOI: 10.1124/dmd.122.000994
This article has not been copyedited and formatted. The final version may differ from this version.

tissue drug distribution has been appreciated and extended to considerations of binding to various tissue components, lipid partitioning, and ionization with further complications produced by differential permeability, convection, and involvement of transporters (Jusko et al., 2020). Further, when assessed for a clearance organ such as liver, it is well appreciated that the occurrence of metabolism causes partial depletion of the tissue making the experimental measurement of K_p subject to the need for a correction factor based on Q_h and CL_{int} (Chen and Gross, 1979; Jeong and Jusko, 2022). Based on an extended WSM, we previously described how the Kp will also differ based on the experimental approach; the single-dose/non-steady-state (SS) K_p will differ from that obtained under SS conditions (K_p^{ss}). It can thus be said that the 'true' K_p of the liver is 'unknowable' owing to the need for a hepatic model that produces a model-dependent CL_{int} value. Ultimately, K_p values for liver can be generated by various means including model-corrected tissue analyses, fitting experimental data (PBPK models), extrapolation from *in vitro* tissue dilution studies, or prediction based on physicochemical properties and tissue composition. They often differ with uncertainties regarding the 'best' value. This work provides an overview of the assumptions, definitions, and mathematical relationships for the three basic hepatic models and assesses their corresponding K_p values relevant to PBPK models using the published single-dose blood/plasma and liver concentration-time data of 14 flow-limited compounds with liver being the primary site of elimination and exhibiting a wide range of hepatic *ER*. The liver K_p of the model compounds were also estimated by the model-fitted tissue/plasma area ratio (AR) (Gallo et al., 1987), Chen & Gross (C&G) (Chen and Gross, 1979) and published *in silico* (Poulin and Theil, 2002a; Poulin and Theil, 2002b; Berezhkovskiy, 2004; Rodgers and Rowland, 2006; Lukacova et al., 2008a; Assmus et al., 2017) methods for comparisons.

Downloaded from dmd.aspetjournals.org at ASPET Journals on April 19, 2024

DMD Fast Forward. Published on October 4, 2022 as DOI: 10.1124/dmd.122.000994
This article has not been copyedited and formatted. The final version may differ from this version.

Theory

The well-acknowledged definition of CL_h is the elimination rate of a drug at steady-state (SS) by the liver divided by the input drug concentration (Rowland, 1972):

$$CL_h = \frac{Elimination\ rate}{C_{in}} = \frac{Q_h(C_{in}-C_{out})}{C_{in}} = Q_h ER \quad (1)$$

where Q_h is liver blood flow, C_{in} and C_{out} are the input and output blood concentrations for the liver, and ER is the hepatic extraction ratio.

In PBPK models, forflow-limited substances, the mass balance for the liver is expressed as:

$$V_h \frac{dC_h}{dt} = Q_h(C_{in} - C_{out}) - f_{uh} CL_{int} C_h \quad (2)$$

where C_h is the measured hepatic drug concentration, V_h is the liver volume, f_{uh} is the unbound fraction in the liver, and CL_{int} is the intrinsic clearance representing the intrinsic ability of the liver to remove the drug. In assuming that the free drug hypothesis applies, the CL_{int} acts upon the unbound hepatic drug concentrations, $C_{uh} = f_{uh}C_h$.

At SS, it can be seen from Eqs. 1 and 2 that:

$$Elimination\ Rate = CL_h C_{in} = CL_{int} C_{uh} \quad (3)$$

where CL_h and C_{in} are usually model-independent for a drug primarily cleared by the liver, while CL_{int} and C_{uh} differ according to the assumed hepatic CL model.

Hepatic Clearance Models

The three basic hepatic CL models (viz. WSM, PTM and DM) along with their assumptions have been described in detail (Rowland et al., 1973; Pang and Rowland, 1977; Roberts and Rowland, 1986a; Roberts and Rowland, 1986b; Pang et al., 2019; Jusko and Li, 2021). Basically, the internal flow pattern of the liver is assumed to differ with different hepatic models. The dispersion number (D_N), which quantifies the degree of axial dispersion of a substance as it transits through the liver is used to differentiate the models.

Downloaded from dmd.aspetjournals.org at ASPET Journals on April 19, 2024

DMD Fast Forward. Published on October 4, 2022 as DOI: 10.1124/dmd.122.000994
This article has not been copyedited and formatted. The final version may differ from this version.

The WSM assumes that the liver is a single and well-stirred compartment with infinite mixing ($D_N = \infty$), which yields a uniform drug concentration in blood throughout the liver. It is identical to that in blood leaving the liver owing to its instantaneous equilibrium with the liver tissue concentration. Therefore:

$$C_{hb,WSM} = C_{out} \tag{4}$$

$$C_{uh,WSM} = C_{uhb,WSM} = f_{uh}C_h = f_{ub}C_{hb,WSM} = f_{ub}C_{out} \tag{5}$$

where $C_{hb,WSM}$ and $C_{uhb,WSM}$ are the total and unbound blood concentrations within the liver for the WSM.

Replacing the $f_{uh}C_h$ term by $f_{ub}C_{out}$ in Eq. 2 under SS conditions gives:

$$Q_h(C_{in} - C_{out}) = f_{ub}CL_{int,WSM}C_{out} \tag{6}$$

and

$$\frac{C_{out}}{C_{in}} = F_h = \frac{Q_h}{Q_h + f_{ub}CL_{int,WSM}} \tag{7}$$

where $CL_{int,WSM}$ is the intrinsic clearance for the WSM, F_h is the hepatic availability of a drug, which also equals the oral bioavailability if the drug is exclusively cleared by the liver.

Thus, for the WSM, the mathematical relationship between ER and $f_{ub}CL_{int,WSM}$ can be expressed according to Eq. 7 as:

$$ER = \frac{f_{ub}CL_{int,WSM}}{Q_h + f_{ub}CL_{int,WSM}} \tag{8}$$

and

$$f_{ub}CL_{int,WSM} = \frac{Q_h ER}{1 - ER} \tag{9}$$

Subsequently, the well-appreciated equation for calculating CL_h based on the WSM is:

$$CL_h = Q_h \frac{f_{ub}CL_{int,WSM}}{Q_h + f_{ub}CL_{int,WSM}} \tag{10}$$

Downloaded from dmd.aspetjournals.org at ASPET Journals on April 19, 2024

DMD Fast Forward. Published on October 4, 2022 as DOI: 10.1124/dmd.122.000994
This article has not been copyedited and formatted. The final version may differ from this version.

The PTM assumes that the liver is comprised of an array of identical and parallel tubes with enzymes distributed evenly in each cross-section of the sinusoidal vascular and perivascular space. No axial spreading ($D_N = 0$) occurs as the drug moves through the liver, resulting in exponentially declining blood concentrations from the inlet to the outlet of the liver. The length-averaged unbound blood concentration in the sinusoid at SS is given by the logarithmic mean of the unbound inlet and outlet concentrations and equals the unbound liver tissue concentration for the PTM:

$$C_{uh,PTM} = C_{uhb,PTM} = \frac{f_{ub}(C_{in}-C_{out})}{ln(\frac{C_{in}}{C_{out}})} \quad (11)$$

and

$$C_{hb,PTM} = \frac{(C_{in}-C_{out})}{ln(\frac{C_{in}}{C_{out}})} \quad (12)$$

where $C_{hb,PTM}$ and $C_{uhb,PTM}$ are the total and unbound blood concentrations within the liver for the PTM.

Under SS, combining Eqs. 2 and 12 gives:

$$Q_h(C_{in} - C_{out}) = f_{ub}CL_{int,PTM}\frac{C_{in}-C_{out}}{\ln(\frac{C_{in}}{C_{out}})} \quad (13)$$

and

$$\frac{C_{out}}{C_{in}} = F_h = e^{-\frac{f_{ub}CL_{int,PTM}}{Q_h}} \quad (14)$$

where $CL_{int,PTM}$ is the intrinsic clearance for the PTM.

Based on Eq. 14, the following equations are applicable to the PTM:

$$ER = 1 - e^{-\frac{f_{ub}CL_{int,PTM}}{Q_h}} \quad (15)$$

$$f_{ub}CL_{int,PTM} = -Q_h ln(1 - ER) \quad (16)$$

Downloaded from dmd.aspetjournals.org at ASPET Journals on April 19, 2024

DMD Fast Forward. Published on October 4, 2022 as DOI: 10.1124/dmd.122.000994
This article has not been copyedited and formatted. The final version may differ from this version.

$$CL_h = Q_h(1 - e^{-\frac{f_{ub}CL_{int,PTM}}{Q_h}}) \quad (17)$$

The internal flow pattern of the DM lies between those of the WSM and the PTM, which assumes a dispersive flow with some extent of longitudinal or axial spreading of a substance during the transit through an organ ($0 < D_N < \infty$). The reported D_N values for liver range from 0.2 to 0.6 (Diaz-Garcia et al., 1992; Chou et al., 1993; Evans et al., 1993; Oliver et al., 2001). The DM is described by a set of second-order partial differential equations that are defined in time and space, and are only solvable after specifying the boundary conditions (Roberts and Rowland, 1986a). Briefly, it has been shown for the DM that the ratio between C_{out} and C_{in} (viz. the hepatic availability F_h) is identical at SS and following a bolus dose based on the closed boundary conditions ($0 < Z < 1$, where Z is defined as the distance along the length of the liver) (Roberts and Rowland, 1986a; Roberts and Rowland, 1986b) which is given by:

$$\frac{C_{out}}{C_{in}} = F_h = \frac{4a}{(1+a)^2 e^{(a-1)/2D_N} - (1-a)^2 e^{-(a+1)/2D_N}} \quad (18)$$

Where $a = (1+4D_N R_N)^{1/2}$, and R_N, the efficiency number that measures the removal rate of substances by liver cells, is given by:

$$R_N = \frac{f_{ub}CL_{int,DM}\rho}{Q_h} \quad (19)$$

where $CL_{int,DM}$ is the intrinsic CL for the DM, ρ is the effective partition coefficient for the unbound drug, defined as:

$$\rho = \frac{P}{P+CL_{int,DM}} \quad (20)$$

where P is the permeability of the drug to the hepatocyte. In the present analysis, the one-compartment DM (e.g., $P >> CL_{int,DM}$ when there is no permeability limitation of the drug to the hepatocyte) was assumed for small-molecule lipophilic drugs; Eq. 19 is thus reduced to:

$$R_N = \frac{f_{ub}CL_{int,DM}}{Q_h} \quad (21)$$

Downloaded from dmd.aspetjournals.org at ASPET Journals on April 19, 2024

DMD Fast Forward. Published on October 4, 2022 as DOI: 10.1124/dmd.122.000994
This article has not been copyedited and formatted. The final version may differ from this version.

Therefore, the *ER* and CL_h for the DM are:

$$ER = 1 - \frac{4a}{(1+a)^2 e^{-(1-a)/2D_N} - (1-a)^2 e^{-(1+a)/2D_N}} \quad (22)$$

$$CL_h = Q_h\left(1 - \frac{4a}{(1+a)^2 e^{-(1-a)/2D_N} - (1-a)^2 e^{-(1+a)/2D_N}}\right) \quad (23)$$

Eq. 22 reduces to Eq. 8 with $D_N = \infty$ for the WSM and to Eq. 15 with $D_N = 0$ for PTM, showing that the WSM and the PTM serve as two extremes of the basic hepatic models with the DM being a more general form.

According to Eq.3, the C_{uh} and C_{uhb} for the DM can be calculated from:

$$C_{uh,DM} = C_{uhb,DM} = \frac{CL_h C_{in}}{CL_{int,DM}} \quad (24)$$

Downloaded from dmd.aspetjournals.org at ASPET Journals on April 19, 2024

DMD Fast Forward. Published on October 4, 2022 as DOI: 10.1124/dmd.122.000994
This article has not been copyedited and formatted. The final version may differ from this version.

Materials and Methods

Assessing Liver CL_{int} and K_p in PBPK Models

Model Compounds and Literature Data Sources

The model compounds were selected based on the following criteria:

- Liver is the major eliminating organ
- Extrahepatic clearances are known or assumed to be negligible
- Absorption rates are high
- ER ranges from low to high
- Time courses of blood/plasma and liver concentrations are available from the literature
- Distribution into the liver and access to the hepatic enzymes are flow-limited (high permeability) with minor or negligible transporter involvements

Upon searching the literature, the measured blood or plasma and liver concentration-time data in rats were found for 14 compounds (tolbutamide (TB), cyclosporine A (CyA), chloroquine (CQ), ethoxybenzamide (EB), fingolimod (FTY720), nicotine (NIC), phenytoin (DPH), diazepam (DZP), propranolol (PPN), pentazocine (PTZ), quinidine (QD), verapamil (VEM), diltiazem (DLZ), and hexobarbital (HB)). Concentration versus time data were digitized from the published graphs in the literature (Tables 1 and 2) using GetData Graph Digitizer version 2.26 (http://getdata-graph-digitizer.com/). All *in vivo* data were obtained from intravenous (IV) bolus studies except that the liver concentration-time profile of CQ was only available after intraperitoneal (IP) bolus administration (Adelusi and Salako, 1982).

Detailed justifications for the selection of model compounds are provided in the Supplemental Methods.

Estimating *in vivo* Liver K_p of Model Compounds by Hepatic Clearance Models

Downloaded from dmd.aspetjournals.org at ASPET Journals on April 19, 2024

DMD Fast Forward. Published on October 4, 2022 as DOI: 10.1124/dmd.122.000994
This article has not been copyedited and formatted. The final version may differ from this version.

A piecewise model fitting approach was adopted in which the blood/plasma concentration time data was fitted first and then used as the forcing input function to characterize the liver concentrations as a single organ. This method, also termed an open-loop method or a forcing function approach, was initially proposed (Ebling et al., 1994) to simulate the disposition of thiopental in the rat and was later applied by others (Foster, 1998; Gueorguieva et al., 2004; Cheung et al., 2018).

Blood/Plasma Concentration-Time Profiles

For compounds without any blood concentrations (C_b) available, their reported plasma concentrations (C_p) were first converted to C_b by multiplying by the blood-to-plasma ratio (R_b) before fitting. The C_b-time data of each drug were fitted by one of the following exponential equations:

$$C_b = \begin{cases} Ae^{-\alpha t} + Be^{-\beta t} \\ Ae^{-\alpha t} + Be^{-\beta t} + Ce^{-\gamma t} \end{cases} \qquad C_{b0} = Dose/V_b \tag{25}$$

where A, B, C are the intercepts, α, β, γ are the slopes, C_{b0} is the initial blood concentration at time 0, and V_b is the average value of the reported blood volumes in the source literature (78 mL/min/kg).

The total blood clearance (CL_b) and ER were estimated from:

$$CL_b = \frac{Dose}{AUC_b} \tag{26}$$

and

$$ER = \frac{CL_b}{Q_h} \tag{27}$$

where AUC_b is the area under the C_b-time curves. Eq. 27 assumed that the liver is the only eliminating organ with $CL_b = CL_h$. Although minor, the contribution of extrahepatic clearance by kidney has been reported for CQ (Liu and Jusko, 2021) and NIC (Plowchalk et al., 1992).

Downloaded from dmd.aspetjournals.org at ASPET Journals on April 19, 2024

DMD Fast Forward. Published on October 4, 2022 as DOI: 10.1124/dmd.122.000994
This article has not been copyedited and formatted. The final version may differ from this version.

Therefore, the CL_h of these two drugs was estimated by subtracting the reported extrahepatic *CL* from CL_b. The reported Q_h values shown in Table 1 were used for *ER* calculation except for VEM and DLZ for which the value of 60.82 mL/min/kg (Brown et al., 1997) was applied due to the unavailability of the reported Q_h. To allow for fair comparisons among different hepatic models, the same Q_h value of 60.82 mL/min/kg was also used for back calculating the $f_{ub}CL_{int}$ associated with each of the hepatic models as well as the subsequent model fittings of liver data. The estimated *ER* for each compound was then fixed and used to obtain the model dependent CL_{int} based on Eq. 9 and 16 for the WSM and PTM, as well as the following equation for the DM based on Eq. 21:

$$f_{ub}CL_{int,DM} = R_N Q_h \tag{28}$$

where R_N was determined from Eq. 22 with a D_N value of 0.6 for the liver (Oliver, 1995; Oliver et al., 2001). The simulated profile of *ER vs* R_N based on Eq. 22 is displayed in Figure S1.

Fitting Liver Concentration-Time Data by Hepatic Clearance Models

Although the assumed internal flow pattern and the resulted unbound tissue and blood concentration within the liver differ, all three basic hepatic clearance models assume perfusion rate-limited distribution and instantaneous equilibrium between the liver tissue C_h (x, t) and blood C_{hb} (x, t) concentration at distance x in the liver and time t for flow-limited substances; therefore, the following relationship applies:

$$C_{hb}(x,t) = \frac{R_b C_h(x,t)}{K_p} \tag{29}$$

where K_p is an apparent value that is also dependent on the assumed hepatic model given the same measured total liver concentration (C_h) owing to the model-dependency of C_{hb}.

Downloaded from dmd.aspetjournals.org at ASPET Journals on April 19, 2024

DMD Fast Forward. Published on October 4, 2022 as DOI: 10.1124/dmd.122.000994
This article has not been copyedited and formatted. The final version may differ from this version.

Since whole liver tissue was collected and homogenized for drug analysis in all the referenced studies, the measured liver concentration at each time point *t* is considered as the tissue space-averaged value. Therefore, Eq. 29 becomes the following for all three hepatic models:

$$C_{hb}(t) = \frac{R_b C_h(t)}{K_p} \tag{30}$$

Combining Eq. 2, 7 and 30, the change of liver concentrations corresponding to the WSM is given by:

$$V_h \frac{dC_h}{dt} = Q_h \left(C_{in} - C_{in} \frac{Q_h}{Q_h + f_{ub} CL_{int,WSM}} \right) - f_{ub} CL_{int,WSM} \frac{R_b C_h}{K_{p,WSM}} \tag{31}$$

where C_{in} is the previous model-fitted C_b of each model compound by Eq. 25, $Q_h C_{in}$ is the forcing input function to fit the liver data and obtain K_p estimates, and V_h was assigned a value of 36.6 mL/kg (Brown et al., 1997). Since the liver data of CQ and CyA had been corrected for residual blood, V_h was adjusted by multiplying the fraction of liver vascular space applied by the source literature (Bernareggi and Rowland, 1991; Kawai et al., 1998; Liu and Jusko, 2021).

Combining Eq. 2, 14 and 30, the concentration changes in the liver corresponding to the PTM are given by:

$$V_h \frac{dC_h}{dt} = Q_h \left(C_{in} - C_{in} e^{-\frac{f_{ub} CL_{int,PTM}}{Q_h}} \right) - f_{ub} CL_{int,PTM} \frac{R_b C_h}{K_{p,PTM}} \tag{32}$$

Combining Eq. 2, 18 and 30, the mass balance of liver corresponding to the DM is described by:

$$V_h \frac{dC_h}{dt} = Q_h \left(C_{in} - C_{in} \frac{4a}{(1+a)^2 e^{(a-1)/2D_N} - (1-a)^2 e^{-(a+1)/2D_N}} \right) - f_{ub} CL_{int,DM} \frac{R_b C_h}{K_{p,DM}} \tag{33}$$

The liver K_p values of all compounds except QD and CQ were estimated by fitting the liver concentration-time profiles using Eq. 31-33. In the case of QD and CQ, nonlinear binding in the liver was reported (Harashima et al., 1985; Liu and Jusko, 2021):

$$C_{bh} = \frac{B_{max} C_{uh}}{K_d + C_{uh}} \tag{34}$$

Downloaded from dmd.aspetjournals.org at ASPET Journals on April 19, 2024

DMD Fast Forward. Published on October 4, 2022 as DOI: 10.1124/dmd.122.000994
This article has not been copyedited and formatted. The final version may differ from this version.

where C_{bh} is the bound concentration of CQ or QD in the liver; C_{uh} and C_h can be calculated from:

$$C_{uh} = C_{uhb} = f_{ub}C_{hb} \tag{35}$$

and

$$C_h = C_{uh} + C_{bh} \tag{36}$$

For simplicity, linear binding of QD in plasma and red blood cells was assumed with the R_b and unbound fraction in the plasma (f_{up}) calculated to be 1.52 and 0.325 (Harashima et al., 1985) (Table S2). Therefore, by combining Eq. 30 and 34-36, the concentration-dependent K_p of CQ and QD is expressed by:

$$K_p = f_{ub}R_b\left(1 + \frac{B_{max}}{K_d + C_{uh}}\right) = f_{up}\left(1 + \frac{B_{max}}{K_d + C_{uh}}\right) \tag{37}$$

where C_{uh} is replaced by Eq. 5 for the WSM, Eq. 11 for the PTM, and Eq. 24 for the DM.

Setting Eq. 31-33 equal to 0 under SS conditions, the K_p associated with each of the hepatic models is:

$$K_{p,WSM} = \frac{C_h^{SS}}{C_{in}^{SS}} R_b \left(\frac{Q_h + f_{ub}CL_{int,WSM}}{Q_h}\right)$$

$$= \frac{C_h^{SS}}{C_p^{SS}} \left(\frac{f_{ub}CL_{int,WSM}}{Q_h ER}\right) \tag{38}$$

$$K_{p,PTM} = \frac{C_h^{SS}}{C_{in}^{SS}} \left(\frac{R_b f_{ub} CL_{int,PTM}}{Q_h \left(1 - e^{-\frac{CL_{int,PTM}}{Q_h}}\right)}\right)$$

$$= \frac{C_h^{SS}}{C_p^{SS}} \left(\frac{f_{ub}CL_{int,PTM}}{Q_h ER}\right) \tag{39}$$

Downloaded from dmd.aspetjournals.org at ASPET Journals on April 19, 2024

DMD Fast Forward. Published on October 4, 2022 as DOI: 10.1124/dmd.122.000994
This article has not been copyedited and formatted. The final version may differ from this version.

$$K_{p,DM} = \frac{C_h^{SS}}{C_{in}^{SS}}\left(\frac{R_b f_{ub} CL_{int,DM}}{Q_h\left(1-\frac{4a}{\frac{(a-1)}{(1+a)^2 e^{2D_N}}-(1-a)^2 e^{-\frac{(a+1)}{2D_N}}}\right)}\right)$$

$$= \frac{C_h^{SS}}{C_p^{SS}}\left(\frac{f_{ub} CL_{int,DM}}{Q_h ER}\right) \quad (40)$$

where C_h^{SS}, C_{in}^{SS} and C_p^{SS} are the liver, blood and plasma concentrations at SS, and the ratio of C_h^{SS} and C_p^{SS} denotes the measured SS K_p (K_p^{SS}).

By replacing the C_h^{SS}/C_p^{SS} terms in Eqs. 38-40 by K_p^{SS}, a general relationship between the PBPK non-SS model-operative liver K_p and the K_p^{SS} applicable to all three hepatic models is:

$$K_P^{SS} = K_p\left(\frac{Q_h ER}{f_{ub} CL_{int}}\right) \quad (41)$$

wherein both K_p and CL_{int} are model-dependent, but jointly produce the model-independent K_p^{SS}. Combining Eq. 8 with Eq. 41, K_p^{SS} can also be expressed as follows for the WSM:

$$K_P^{SS} = K_{p,WSM}\left(1-\frac{f_{ub} CL_{int,WSM}}{Q_h + f_{ub} CL_{int,WSM}}\right) = K_{p,WSM}(1-ER) \quad (42)$$

Model Fitting

The model fittings of blood and liver concentration-time data were performed by nonlinear regression using the maximum likelihood algorithm in ADAPT 5 (Biomedical Simulations Resources, Los Angeles, CA) (D'Argenio et al., 2009). The variance model used was:

$$V_i = \left(\sigma_{inter} + \sigma_{slope} Y_i\right)^2 \quad (43)$$

where V_i is the variance of the ith data point; Y_i is the ith model-predicted concentration; σ_{inter} and σ_{slope} are the variance model parameters. Model selection was based on the goodness-of-fit criteria, which included the Akaike Information Criterion (AIC), visual inspection of the fitted profiles, and CV% of the parameter estimates.

The ADAPT code for the model for one compound is provided in the Supplemental Methods.

Downloaded from dmd.aspetjournals.org at ASPET Journals on April 19, 2024

DMD Fast Forward. Published on October 4, 2022 as DOI: 10.1124/dmd.122.000994
This article has not been copyedited and formatted. The final version may differ from this version.

Liver K_p of Model Compounds Obtained by Other Methods

The liver K_p values were also calculated as follows for comparisons with those estimated by the hepatic clearance models:

1. Reported K_p^{ss} calculated as the SS liver-to-plasma concentration ratio (Table 1).
2. Apparent K_p values calculated from the AR method (Gallo et al., 1987):

$$K_{p,AR} = \frac{AUC_{h,pred}}{AUC_{p,pred}} \quad (44)$$

where $AUC_{h,pred}$ and $AUC_{p,pred}$ are the areas under the hepatic clearance model-predicted liver and plasma curves (from time 0 to infinity).

3. Apparent K_p values obtained from the terminal slopes of C_h- and C_p-time data of the model compounds according to the C&G method (Chen and Gross, 1979) for the liver:

$$K_{p,C\&G} = \frac{(Q_h+CL_{int,WSM})\frac{C_h^0}{C_p^0}}{Q_h+V_{SP}\lambda_{zSP}\frac{C_{SP}^0}{C_p^0}+V_G\lambda_{zG}\frac{C_G^0}{C_p^0}+V_h\lambda_{zh}\frac{C_h^0}{C_p^0}} \quad (45)$$

where C^0 and λ_z are the intercept and slope of the terminal elimination phase of the plasma or tissue concentration-time curve and subscripts *SP* and *G* refer to the spleen and gut if available with the assumptions that no metabolism occurs in these two organs. According to Eq.13 in (Jeong and Jusko, 2022) and the above Eq. 44 (Chen and Gross, 1979), the K_p^{ss} for flow-limited substances can be obtained from $K_{p,C\&G}$ in a similar way as the WSM:

$$K_P^{ss} = K_{p,C\&G}\left(1-\frac{f_{ub}CL_{int,WSM}}{Q_h+f_{ub}CL_{int,WSM}}\right) = K_{p,C\&G}(1-ER) \quad (46)$$

4. Apparent K_p predicted by the *in silico* methods implemented in the GastroPlus PBPK Simulator (Version 9.8.0002; Simulation Plus Inc., Lancaster, CA) based on the published methods (Poulin and Theil, 2002a; Poulin and Theil, 2002b) (M1), (Berezhkovskiy, 2004) (M2), (Rodgers and Rowland, 2006) (M3), and (Lukacova et al.,

Downloaded from dmd.aspetjournals.org at ASPET Journals on April 19, 2024

DMD Fast Forward. Published on October 4, 2022 as DOI: 10.1124/dmd.122.000994
This article has not been copyedited and formatted. The final version may differ from this version.

2008a) (M4 for all compounds except for CQ). For CQ, M4 refers to the extended Lukacova method that includes lysosomal trapping for basic compounds (Assmus et al., 2017).

Downloaded from dmd.aspetjournals.org at ASPET Journals on April 19, 2024

DMD Fast Forward. Published on October 4, 2022 as DOI: 10.1124/dmd.122.000994
This article has not been copyedited and formatted. The final version may differ from this version.

Results

Signature Profiles of CL_h, CL_{int}, K_p in Relation to *ER*

Model simulations were performed using Eq. 1 for CL_h, Eq. 9, 16, and 28 for each model CL_{int}, and Eq. 38-40 for each model K_p (assuming f_{ub} and R_b all equal to 1) with *ER* increasing from 0 to 1 to examine the general trend and model-dependencies of these parameters. As shown in Figure 1A, CL_h increased with increasing *ER* with the upper limit being Q_h. The CL_{int} of all hepatic models can exceed Q_h, with the rank order being $CL_{int,WSM} > CL_{int,DM} > CL_{int,PTM}$ given the same *ER*. At the low *ER* range (e.g., 0-0.3), the CL_{int} values of all models are similar and close to the CL_h. However, larger differences in CL_{int} were observed at the medium to high *ER* values (e.g., 0.3 to 1). Like the model-dependent CL_{int}, the PBPK-operative K_p also showed increasing trends with increased *ER* and displayed hepatic model-dependency (Figure 1B), with the WSM K_p being the largest and the PTM K_p being the smallest. The K_p of all three models are close to or larger than the assumed SS K_p value due to different extents of hepatic elimination. For low *ER* drugs, the hepatic model-specific K_p values are comparable to the SS K_p while larger deviations were seen for high *ER* drugs.

Liver K_p of the Model Compounds

In applying the hepatic clearance models by the open loop approach, the blood PK data of the model compounds were first fitted by the exponential functions (Eq. 25), with CL_b, *ER* and $f_{ub}CL_{int}$ estimated as secondary parameters based on Eq. 9, 16, and 26-28. These PK parameter estimates are presented in Tables 2 and S1 and the model fittings are displayed in Figure 2. As can be seen, there is good agreement between the observations and model predictions of blood concentrations and the fitted parameters exhibit low CV% values. The C_b-time data of CQ after an IP dose were better fitted without an absorption phase as presented. In general, the estimated

Downloaded from dmd.aspetjournals.org at ASPET Journals on April 19, 2024

DMD Fast Forward. Published on October 4, 2022 as DOI: 10.1124/dmd.122.000994
This article has not been copyedited and formatted. The final version may differ from this version.

CL_b and ER values were comparable to those reported/calculated except that the estimated values were lower for CQ, PTZ, QD and PPN. The estimated CL_{int} values exhibited hepatic model-dependency and increased with increasing ER, consistent with the expectations of the CL_{int} profiles shown in Figure 1A.

The unbound blood/tissue concentrations within the liver related to each of the hepatic models were simulated according to Eq. 5, 11, and 24 using VEM as an example (Figure 3). Consistent with theoretical expectations, model-dependencies are observed with the WSM exhibiting the lowest concentrations while those of the PTM are the highest. The unbound liver blood concentrations of all hepatic models are lower than the observed blood concentrations due to depletion by hepatic clearance even when f_{ub} was assumed to be 1. It can be noted that, just as the plasma AUC is determined by Dose/systemic clearance, the hepatic free AUC is determined by Dose/intrinsic clearance. Of course, the latter is model-dependent as shown while the former is not.

Next, the *in vivo* fitted liver K_p values of the model compounds were estimated by applying the WSM, PTM and DM to the measured liver concentration-time data using the previously model-fitted blood concentration-time data as the forcing input function. The liver K_p and nonlinear tissue binding-related parameters (B_{max} and K_d) of QD and CQ were estimated with reasonable CV% values (Table 3) and the liver concentration-time profiles of all compounds were well captured (Figure 2) except for some underpredictions for the early data points of EB and CyA. Nonlinear tissue binding reasonably explained the slower terminal decline in the liver concentrations of QD and CQ as compared to their blood concentrations. Like the CL_{int}, the PBPK-operative K_p also differs for the hepatic models with the WSM yielding the highest value while the PTM gives the lowest. Such model-dependency is unnoticeable for low ER drugs but

Downloaded from dmd.aspetjournals.org at ASPET Journals on April 19, 2024

DMD Fast Forward. Published on October 4, 2022 as DOI: 10.1124/dmd.122.000994
This article has not been copyedited and formatted. The final version may differ from this version.

becomes more remarkable as *ER* increases. It is evident that the predicted liver concentrations as fitted by different hepatic models were identical although the CL_{int} and K_p values differ.

The apparent liver K_p values were also obtained by the AR and C&G methods (Table 3) and compared with those estimated by the WSM (Figure 4). It is important to appreciate the different methods used for estimating K_p values. The $K_{p,C\&G}$ values that were corrected for hepatic extraction based on the WSM are comparable with the $K_{p,WSM}$ for most compounds. The $K_{p,AR}$ are uncorrected values that exhibit larger deviations from $K_{p,WSM}$ and $K_{p,C\&G}$ as the contribution of hepatic extraction increases. The experimental and GastroPlus-predicted physicochemical properties of all model compounds are summarized in Table S2 and were used for predicting the *in silico* K_p ($K_{p,exp}$ and $K_{p,pred}$) by the M1 through M4 methods, with the results shown in Table 4 and compared in Figure S2. In general, the predictions by M1 and M2 are similar, while those obtained by M3 and M4 are close to each other. The *in silico* $K_{p,pred}$ are generally in line with the $K_{p,exp}$ except for those of CQ, HB, CYA and NIC calculated by M3 and M4, and those of DPH predicted by all *in silico* methods. Overall, regardless of which *in silico* method was used, the $K_{p,pred}$ and $K_{p,exp}$ differ appreciably from the WSM K_p for most of the compounds (Figure 4).

Comparisons of the Predicted and Reported Liver K_p^{ss}

To allow for more intuitive comparisons among different prediction methods, the K_p obtained by the hepatic clearance model fittings, C&G method, and *in silico* methods were converted to their corresponding uncorrected K_p^{ss} using Eq. 41, 42 and 46. With the model-specific sets of CL_{int} and K_p, different hepatic models yielded the same K_p^{ss} as expected (Eq. 41). Therefore, a single K_p^{ss} value was listed for all the compounds (Table 3). As can be seen from Figure 5A, the AR K_p and the hepatic model-predicted K_p^{ss} and the C&G method are comparable and within a 2-fold range from the reported *in vivo* K_p^{ss} for all compounds except for slight underpredictions for PPN

Downloaded from dmd.aspetjournals.org at ASPET Journals on April 19, 2024

DMD Fast Forward. Published on October 4, 2022 as DOI: 10.1124/dmd.122.000994
This article has not been copyedited and formatted. The final version may differ from this version.

(predicted/reported K_p^{ss} ratio: 0.34~0.42). In contrast, the *in silico* methods performed poorly (more than 2-fold difference) for most of the compounds with either experimental (Figure 5B) or predicted (Figure 5C) drug properties. Nevertheless, the *in silico* methods performed slightly better when combined with the experimental drug properties, which generated K_p^{ss} predictions within the 2-fold range for TB (M3 and M4), HB (all *in silico* methods), DPH (all *in silico* methods), NIC (M3), PPN (M2) and DZP (M1).

Owing to the nonlinearity in tissue binding, the K_p^{ss} of CQ and QD obtained by different methods were compared separately in Figure S3. The reported and hepatic model predicted K_p^{ss} of CQ and QD were simulated using their corresponding B_{max} and K_d values according to Eq. 5, 7, 25, 37, and 42 with the plasma concentration range of 5~200 ng/mL for CQ and 0.7~5 μg/mL for QD. For CQ, lysosomal trapping along with the appreciable binding to acidic phospholipids in cell membranes have been reported (Allison and Young, 1964; Tietz et al., 1990; Zheng et al., 2011), which are major contributors to the extensive tissue distribution and long terminal half-life of this basic lipophilic molecule. Thus, M4 (Lukacova et al., 2008a) extended with the inclusion of lysosomal sequestration (Assmus et al., 2017) was used specifically for CQ. As shown in Figure S3, the hepatic clearance models slightly underpredict the K_p^{ss} of CQ, with the model-predicted *vs* reported K_p^{ss} ratio ranging from 0.24~0.48 within the simulated C_p range. With the incorporation of lysosomal trapping, the *in silico* M4 combined with the experimental drug properties yielded the best K_p^{ss} predictions for CQ among all the methods, followed by the C&G and AR methods, and the *in silico* M3 with the experimental drug properties. The M4 method overpredicted the K_p^{ss} of CQ when the predicted physicochemical properties were used. The reported K_p^{ss} value of CQ measured at the C_p^{ss} of 157 ng/mL (Earle et al., 1948) is about 6-fold higher than that simulated based on the reported tissue binding parameters (Liu and Jusko,

Downloaded from dmd.aspetjournals.org at ASPET Journals on April 19, 2024

DMD Fast Forward. Published on October 4, 2022 as DOI: 10.1124/dmd.122.000994
This article has not been copyedited and formatted. The final version may differ from this version.

2021) at the same C_p^{ss}. In contrast, the hepatic models yielded good K_p^{ss} predictions for QD within the analyzed C_p range. Among all the other methods, the *in silico* M3 and M4 methods combined with the experimental drug properties also performed reasonably well for predicting the K_p^{ss} of QD. The effects of improper use of K_p on the prediction of liver concentration-time profiles by the WSM were demonstrated using DLZ as an example. Model simulations were performed by decreasing or increasing the previously fitted $K_{p,WSM}$ to ±2- and 5-fold its normal value, and also with the lowest and highest *in silico* K_p values (i.e., M1 $K_{p,exp}$ of 4.33, and M3 $K_{p,pred}$ of 14.82) (Table 4). As shown in Figure 6, the direct use of a correct $CL_{int,WSM}$ with K_p obtained from sources other than fitting the same *in vivo* data may result in various degrees of under- and over-predictions of the liver concentrations.

Downloaded from dmd.aspetjournals.org at ASPET Journals on April 19, 2024

DMD Fast Forward. Published on October 4, 2022 as DOI: 10.1124/dmd.122.000994
This article has not been copyedited and formatted. The final version may differ from this version.

Discussion

The metabolic and biliary excretory capabilities of the liver are fundamental biochemical activities that determine elimination rates of drugs in the complex anatomical and physiological functioning of the hepatic system. Likewise, drugs are 'bound' in the liver by multiple mechanisms including reversible and irreversible attachment to macromolecules, lipid partitioning, and ion trapping with differential blood/tissue permeability, transport and convection rates often adding complications (Jusko et al., 2020). The simplest net expression of these complex drug- and organ-specific processes utilized in PK are the organ space-average CL_{int} and K_P values. Attempts to measure these properties using *in vitro* methods unfortunately require a PK model of the liver for *in vivo* extrapolation (IVIVE). While numerous hepatic clearance models exist, the simple WSM is most commonly utilized in both IVIVE and PBPK. This report explores and compares the operation of the WSM, PTM, and DM in PBPK modeling with a particular focus on resultant K_P values. An overview of the theoretical concepts and mathematical relationships applicable to the basic hepatic models in context of PBPK was presented. The model-dependencies in liver CL_{int} have long been appreciated while the properties of the PBPK-operative K_p were explored further and shown to differ among the hepatic models using experimental published data for 14 model compounds and by assessing *in silico* methodology.

The open-loop approach where the blood/plasma data were pre-fitted and fixed was advantageous for our purposes as we did not have to deal with involvement of organs/tissues other than the liver. When applying the exponential functions to describe the blood PK data, the initial blood concentration was fixed to Dose/V_b so that the initial distribution space is the blood volume (V_b) to create a physiologically plausible initial decline of drug concentrations that

Downloaded from dmd.aspetjournals.org at ASPET Journals on April 19, 2024

DMD Fast Forward. Published on October 4, 2022 as DOI: 10.1124/dmd.122.000994
This article has not been copyedited and formatted. The final version may differ from this version.

mimics the behavior of full PBPK models as compared to estimating an initial distribution space as with compartment models. This open-loop method was reported to generate comparable K_p estimates as obtained by fitting all tissues simultaneously using a full PBPK model (Gueorguieva et al., 2004). However, the limitation with this approach is that the CL_{int} is highly correlated with K_p resulting in extremely large CV% values when both parameters are estimated simultaneously. In the present analysis the hepatic model-specific CL_{int} was first estimated from the CL_b or ER by fitting the blood PK data knowing or assuming that the liver is the only clearance organ and then fixed to only estimate the PBPK-operative K_p. The calculations of $CL_{int,WSM}$ and $CL_{int,PTM}$ were straightforward (Eq. 9 and 16), while the DM has no explicit solution for the $CL_{int,DM}$ and thus was indirectly calculated (Eq. 28). It was feasible to obtain R_N from a range of ER values with a pre-set D_N value by model simulations using Eq. 22 (see Figure S1) as was similarly done previously (Oliver et al., 2001). The D_N value of 0.6 based on the closed boundary conditions (Oliver, 1995; Oliver et al., 2001) gave reasonable predictions of hepatic availability corresponding to the PTM and WSM extremes when D_N approaches to 0 and infinity as compared to the open or mixed boundary conditions (Roberts and Rowland, 1986a; Roberts and Rowland, 1986b). Reported Q_h values in the literature and commercial software range from 47 to 85 mL/min/kg (Table 1). To make fair comparisons among the models, the Q_h of 60.82 mL/min/kg was chosen (Brown et al., 1997), which is close to the median value of the reported Q_h range used to calculate the model-specific CL_{int} values for all compounds and also used in fitting of liver data. The hepatic model-dependencies in the estimated CL_{int} occurred as expected and are most remarkable for drugs with high ER. We show that the PBPK-operative K_p is also dependent on the hepatic model, with the same rank order as for CL_{int}. It is expected that if the

Downloaded from dmd.aspetjournals.org at ASPET Journals on April 19, 2024

DMD Fast Forward. Published on October 4, 2022 as DOI: 10.1124/dmd.122.000994
This article has not been copyedited and formatted. The final version may differ from this version.

lower PTM or DM K_p value was applied to model fittings based on the WSM, the liver concentrations would be underestimated (Figure 6).

Besides being estimated by fitting plasma and liver profiles with PBPK models, K_p was obtained by several other means. Using the ratio of SS tissue-to-plasma concentration by constant IV infusion studies or from the tissue/plasma area ratio (AR) from IV bolus studies does not make any assumptions about the tissue model structure and the resulting K_p values are equivalent for non-eliminating tissues under linear PK conditions. However, for the liver, the experimentally measured K_p differs from the (unknown) true value and needs to be corrected before utilization in PBPK models. The usual approach for such purpose is application of the WSM CL_{int} (Houston, 1994) that was presumably done as the basis of the *in silico* prediction methods. During early drug development when there are no *in vivo* measurements available, K_p can also be predicted using *in silico* quantitative structure-property relationships (QSPR) combined with tissue composition properties using the cited published methods and found in commercial software such as the GastroPlus Simulator (Other software such as SimCyp and PKSim also offer most of these methods.). In this work, the apparent liver K_p values of all model compounds were calculated using *in silico* methods. Overall, there were little differences in the K_p based on *in vivo* measurements (e.g., hepatic models, AR, and C&G methods) when the *ER* is low, while the $K_{p,AR}$ is smaller than those estimated by the other two methods as *ER* increases due to the lack of correction for hepatic elimination. With *in silico* approaches, compound-specific input parameters (e.g., pKa, *Log*P, R_b, and f_{up}) play important roles in making K_p predictions. Using experimental and QSPR-predicted physicochemical properties produced comparable *in silico* K_p values. The adjusted f_{up} that improves K_p predictions of highly lipophilic compounds (Lukacova et al., 2008b) was used. The *in silico* predicted K_p values were compared with the WSM K_p since

Downloaded from dmd.aspetjournals.org at ASPET Journals on April 19, 2024

DMD Fast Forward. Published on October 4, 2022 as DOI: 10.1124/dmd.122.000994
This article has not been copyedited and formatted. The final version may differ from this version.

they are often utilized in PBPK models with CL_{int} either obtained from *in vitro* or back calculated from the *in vivo* CL_h using the WSM to predict tissue drug disposition. The correlation between the *in silico* and WSM K_p values was not very good for most compounds (Figure 4). Poor agreement was also found for dexamethasone (Song et al., 2020), CQ (Liu and Jusko, 2021), prednisolone (Li et al., 2020), and for many additional compounds (Jeong and Jusko, 2022). Directly using the *in silico* K_p with a WSM CL_{int} may result in poor predictions for the liver concentrations (Figure 6). As shown (Lukacova et al., 2008a), the *in silico* K_p predictions should only be considered approximate. Values for liver are even more prone to error than other tissues owing to the need for correction of measured values for CL_{int}.

The limitations of this study are the use of published digitized data and that only the three basic hepatic models assuming perfusion-limitations were compared. Later hepatic models have been expanded to include influences of cell permeability and transporter-mediated clearances (Miyauchi et al., 1987; Kwon and Morris, 1997; Sirianni and Pang, 1997, Jeong and Jusko, 2022). Second-order partial differential equations involving both space and time as needed for the DM (Oliver, 1995; Oliver et al., 2001) were not considered in this analysis since the observed total liver concentration at each time point for all of the study drugs is the tissue space-averaged value. An alternative hepatic model called the series-compartment model was reported to closely approximate the DM where the liver is divided into several compartments connected by blood flow in tandem (Gray and Tam, 1987). It was later extended by considering the hepatic zonation of metabolizing enzymes/transporters (Tirona and Pang, 1996; Abu-Zahra and Pang, 2000) and transporter-associated clearances (Watanabe et al., 2009; Jones et al., 2012; Li et al., 2014; Morse et al., 2017). The assumption that the liver is the only clearance organ may not be perfectly true for some of the selected compounds. However, the main objective of this work is

Downloaded from dmd.aspetjournals.org at ASPET Journals on April 19, 2024

DMD Fast Forward. Published on October 4, 2022 as DOI: 10.1124/dmd.122.000994
This article has not been copyedited and formatted. The final version may differ from this version.

to assess the hepatic model-dependencies of CL_{int} and the PBPK-operative K_p, and how they change with changing *ER*. In any case, if the liver is not fully the elimination organ, the relative values of K_p obtained using the three hepatic models will still differ with the same trend.

Considerable attention has been paid to assessing data from isolated hepatic perfusion studies to identify the "best" model for hepatic clearance (Sodhi et al., 2020), but such assessments have seldom if ever been made using data from PBPK studies. Our report demonstrates how to do this and reveals that the three basic hepatic models that assume different internal concentrations produce differing operative CL_{int} and K_p values especially for drugs with high *ER* in PBPK-type studies. However, all three models appear to fit liver PK data equally well and such quality of fittings does not serve to discriminate the 'correct' model, at least for flow-limited substances. Our findings are most relevant when using these hepatic models for IVIVE where a model-dependent CL_{int} is needed to correct measured tissue concentrations for depletion by metabolism with the WSM requiring the largest correction factor. Perhaps use of the PTM or DM that entail smaller adjustments would reduce any errors in such corrections. The hepatic model-dependency may also have an impact when assessing the PK/pharmacodynamic relationships when effects relate to assumed hepatic concentrations. Differences in hepatic exposures of presumed unbound drug were found to relate to the expected Dose/intrinsic clearance values (Figure 3).

Downloaded from dmd.aspetjournals.org at ASPET Journals on April 19, 2024

DMD Fast Forward. Published on October 4, 2022 as DOI: 10.1124/dmd.122.000994
This article has not been copyedited and formatted. The final version may differ from this version.

Authorship Contributions

Participated in research design: Li and Jusko.

Performed data analysis: Li.

Wrote or contributed to the writing of the manuscript: Li and Jusko.

Downloaded from dmd.aspetjournals.org at ASPET Journals on April 19, 2024

DMD Fast Forward. Published on October 4, 2022 as DOI: 10.1124/dmd.122.000994
This article has not been copyedited and formatted. The final version may differ from this version.

References

Abu-Zahra TN and Pang KS (2000) Effect of zonal transport and metabolism on hepatic removal: enalapril hydrolysis in zonal, isolated rat hepatocytes in vitro and correlation with perfusion data. *Drug Metab Dispos* **28:**807-813.

Adelusi SA and Salako LA (1982) Kinetics of the distribution and elimination of chloroquine in the rat. *Gen Pharmacol* **13:**433-437.

Allison AC and Young MR (1964) Uptake of dyes and drugs by living cells in culture. *Life Sci (1962)* **3:**1407-1414.

Assmus F, Houston JB, and Galetin A (2017) Incorporation of lysosomal sequestration in the mechanistic model for prediction of tissue distribution of basic drugs. *Eur J Pharm Sci* **109:**419-430.

Bass L, Keiding S, Winkler K, and Tygstrup N (1976) Enzymatic elimination of substrates flowing through the intact liver. *J Theor Biol* **61:**393-409.

Benet LZ, Liu S, and Wolfe AR (2018) The universally unrecognized assumption in predicting drug clearance and organ extraction ratio. *Clin Pharmacol Ther* **103:**521-525.

Berezhkovskiy LM (2004) Volume of distribution at steady state for a linear pharmacokinetic system with peripheral elimination. *J Pharm Sci* **93:**1628-1640.

Bernareggi A and Rowland M (1991) Physiologic modeling of cyclosporin kinetics in rat and man. *J Pharmacokinet Biopharm* **19:**21-50.

Brown RP, Delp MD, Lindstedt SL, Rhomberg LR, and Beliles RP (1997) Physiological parameter values for physiologically based pharmacokinetic models. *Toxicol Ind Health* **13:**407-484.

Chen HS and Gross JF (1979) Estimation of tissue-to-plasma partition coefficients used in physiological pharmacokinetic models. *J Pharmacokinet Biopharm* **7:**117-125.

Cheung SYA, Rodgers T, Aarons L, Gueorguieva I, Dickinson GL, Murby S, Brown C, Collins B, and Rowland M (2018) Whole body physiologically based modelling of beta-blockers in the rat: events in tissues and plasma following an i.v. bolus dose. *Br J Pharmacol* **175:**67-83.

Chou CH, Evans AM, Fornasini G, and Rowland M (1993) Relationship between lipophilicity and hepatic dispersion and distribution for a homologous series of barbiturates in the isolated perfused in situ rat liver. *Drug Metab Dispos* **21:**933-938.

D'Argenio D, Schumitzky A, and Wang X (2009) *Adapt 5 User's Guide: Pharmacokinetic/Pharmacodynamic Systems Analysis Software.* BMSR, University of Southern California.

Diaz-Garcia JM, Evans AM, and Rowland M (1992) Application of the axial dispersion model of hepatic drug elimination to the kinetics of diazepam in the isolated perfused rat liver. *J Pharmacokinet Biopharm* **20:**171-193.

Earle DP, Berliner RW, Taggart JV, Welch WJ, Zubrod CG, Wise NB, Chalmers TC, Greif RL, and Shannon JA (1948) Studies on the chemotherapy of the human malarias. Ii. Method for the quantitative assay of suppressive antimalarial action in falciparum malaria. *J Clin Invest* **27:**75-79.

Ebling WF, Wada DR, and Stanski DR (1994) From piecewise to full physiologic pharmacokinetic modeling: Applied to thiopental disposition in the rat. *J Pharmacokinet Biopharm* **22:**259-292.

Evans AM, Hussein Z, and Rowland M (1993) Influence of albumin on the distribution and elimination kinetics of diclofenac in the isolated perfused rat liver: Analysis by the impulse-response technique and the dispersion model. *J Pharm Sci* **82:**421-428.

Foster DM (1998) Developing and testing integrated multicompartment models to describe a single-input multiple-output study using the SAAM II software system. *Adv Exp Med Biol* **445:**59-78.

Fujio I, Koichi Y, Tsukinaka Y, Akira T, and Yuzo M (1983) Physiological pharmacokinetic model for pentazocine. I. Tissue distribution and elimination in the rat. *Int J Pharm* **15:**321-333.

Downloaded from dmd.aspetjournals.org at ASPET Journals on April 19, 2024

DMD Fast Forward. Published on October 4, 2022 as DOI: 10.1124/dmd.122.000994
This article has not been copyedited and formatted. The final version may differ from this version.

Gallo JM, Lam FC, and Perrier DG (1987) Area method for the estimation of partition coefficients for physiological pharmacokinetic models. *J Pharmacokinet Biopharm* **15:**271-280.

Gillette JR (1971) Factors affecting drug metabolism. *Ann N Y Acad Sci* **179:**43-66.

Gray MR and Tam YK (1987) The series-compartment model for hepatic elimination. *Drug Metab Dispos* **15:**27-31.

Gueorguieva I, Nestorov IA, Murby S, Gisbert S, Collins B, Dickens K, Duffy J, Hussain Z, and Rowland M (2004) Development of a whole body physiologically based model to characterise the pharmacokinetics of benzodiazepines. 1: Estimation of rat tissue-plasma partition ratios. *J Pharmacokinet Pharmacodyn* **31:**269-298.

Hallifax D, Foster JA, and Houston JB (2010) Prediction of human metabolic clearance from in vitro systems: Retrospective analysis and prospective view. *Pharm Res* **27:**2150-2161.

Harashima H, Sawada Y, Sugiyama Y, Iga T, and Hanano M (1985) Analysis of nonlinear tissue distribution of quinidine in rats by physiologically based pharmacokinetics. *J Pharmacokinet Biopharm* **13:**425-440.

Houston JB (1994) Utility of in vitro drug metabolism data in predicting in vivo metabolic clearance. *Biochem Pharmacol* **47:**1469-1479.

Houston JB and Carlile DJ (1997) Prediction of hepatic clearance from microsomes, hepatocytes, and liver slices. *Drug Metab Rev* **29:**891-922.

Igari Y, Sugiyama Y, Awazu S, and Hanano M (1982) Comparative physiologically based pharmacokinetics of hexobarbital, phenobarbital and thiopental in the rat. *J Pharmacokinet Biopharm* **10:**53-75.

Igari Y, Sugiyama Y, Sawada Y, Iga T, and Hanano M (1983) Prediction of diazepam disposition in the rat and man by a physiologically based pharmacokinetic model. *J Pharmacokinet Biopharm* **11:**577-593.

Igari Y, Sugiyama Y, Sawada Y, Iga T, and Hanano M (1984) In vitro and in vivo assessment of hepatic and extrahepatic metabolism of diazepam in the rat. *J Pharm Sci* **73:**826-828.

Ito K and Houston JB (2004) Comparison of the use of liver models for predicting drug clearance using in vitro kinetic data from hepatic microsomes and isolated hepatocytes. *Pharm Res* **21:**785-792.

Itoh T, Sawada Y, Lin TH, Iga T, and Hanano M (1988) Kinetic analysis of phenytoin disposition in rats with experimental renal and hepatic diseases. *J Pharmacobiodyn* **11:**289-308.

Iwatsubo T, Hirota N, Ooie T, Suzuki H, Shimada N, Chiba K, Ishizaki T, Green CE, Tyson CA, and Sugiyama Y (1997) Prediction of in vivo drug metabolism in the human liver from in vitro metabolism data. *Pharmacol Ther* **73:**147-171.

Jeong YS and Jusko WJ (2022) Consideration of fractional distribution parameter fd in the chen and gross method for tissue-to-plasma partition coefficients: Comparison of several methods. *Pharm Res* **39:**463-479.

Jones HM, Barton HA, Lai Y, Bi YA, Kimoto E, Kempshall S, Tate SC, El-Kattan A, Houston JB, Galetin A, and Fenner KS (2012) Mechanistic pharmacokinetic modeling for the prediction of transporter-mediated disposition in humans from sandwich culture human hepatocyte data. *Drug Metab Dispos* **40:**1007-1017.

Jusko WJ and Li X (2021) Assessment of the Kochak-Benet equation for hepatic clearance for the parallel-tube model: Relevance of classic clearance concepts in PK and PBPK. *AAPS J* **24:**5.

Jusko WJ, Molins EAG, and Ayyar VS (2020) Seeking Nonspecific Binding: Assessing the Reliability of Tissue Dilutions for Calculating Fraction Unbound. *Drug Metab Dispos* **48:**894-902.

Kawai R, Mathew D, Tanaka C, and Rowland M (1998) Physiologically based pharmacokinetics of cyclosporine A: Extension to tissue distribution kinetics in rats and scale-up to human. *J Pharmacol Exp Ther* **287:**457-468.

Kilford PJ, Stringer R, Sohal B, Houston JB, and Galetin A (2009) Prediction of drug clearance by glucuronidation from in vitro data: Use of combined cytochrome P450 and UDP-

Downloaded from dmd.aspetjournals.org at ASPET Journals on April 19, 2024

DMD Fast Forward. Published on October 4, 2022 as DOI: 10.1124/dmd.122.000994
This article has not been copyedited and formatted. The final version may differ from this version.

glucuronosyltransferase cofactors in alamethicin-activated human liver microsomes. *Drug Metab Dispos* **37:**82-89.

Kwon Y and Morris ME (1997) Membrane transport in hepatic clearance of drugs. I: Extended hepatic clearance models incorporating concentration-dependent transport and elimination processes. *Pharm Res* **14:**774-779.

Lewis AE (1948) The concept of hepatic clearance. *Am J Clin Pathol* **18:**789-795.

Li R, Barton HA, Yates PD, Ghosh A, Wolford AC, Riccardi KA, and Maurer TS (2014) A "middle-out" approach to human pharmacokinetic predictions for OATP substrates using physiologically-based pharmacokinetic modeling. *J Pharmacokinet Pharmacodyn* **41:**197-209.

Li X, DuBois DC, Almon RR, and Jusko WJ (2020) Physiologically based pharmacokinetic modeling involving nonlinear plasma and tissue binding: Application to prednisolone and prednisone in rats. *J Pharmacol Exp Ther* **375:**385-396.

Lin JH, Hayashi M, Awazu S, and Hanano M (1978) Correlation between in vitro and in vivo drug metabolism rate: oxidation of ethoxybenzamide in rat. *J Pharmacokinet Biopharm* **6:**327-337.

Lin JH, Sugiyama Y, Awazu S, and Hanano M (1982) In vitro and in vivo evaluation of the tissue-to-blood partition coefficient for physiological pharmacokinetic models. *J Pharmacokinet Biopharm* **10:**637-647.

Liu X and Jusko WJ (2021) Physiologically based pharmacokinetics of lysosomotropic chloroquine in rat and human. *J Pharmacol Exp Ther* **376:**261-272.

Lukacova V, Parrott N, Lavé T, Fraczkiewicz G, Bolger M, and Woltosz W (2008a) General approach to calculation of tissue:plasma partition coefficients for physiologically based pharmacokinetic (PBPK) modeling, in: *AAPS National Annual Meeting and Exposition*, Atlanta, GA.

Lukacova V, Parrott N, Lavé T, Fraczkiewicz G, Bolger M, and Woltosz W (2008b) Role of fraction unbound in plasma in calculations of tissue:plasma partition coefficients, in: *American Association of Pharmaceutical Scientists (AAPS)*, Atlanta, GA.

Meno-Tetang GM, Li H, Mis S, Pyszczynski N, Heining P, Lowe P, and Jusko WJ (2006) Physiologically based pharmacokinetic modeling of FTY720 (2-amino-2[2-(-4-octylphenyl)ethyl]propane-1,3-diol hydrochloride) in rats after oral and intravenous doses. *Drug Metab Dispos* **34:**1480-1487.

Miller NA, Reddy MB, Heikkinen AT, Lukacova V, and Parrott N (2019) Physiologically based pharmacokinetic modelling for first-in-human predictions: An updated model building strategy illustrated with challenging industry case studies. *Clin Pharmacokinet* **58:**727-746.

Miyauchi S, Sugiyama Y, Sawada Y, Morita K, Iga T, and Hanano M (1987) Kinetics of hepatic transport of 4-methylumbelliferone in rats. Analysis by multiple indicator dilution method. *J Pharmacokinet Biopharm* **15:**25-38.

Morse BL, MacGuire JG, Marino AM, Zhao Y, Fox M, Zhang Y, Shen H, Griffith Humphreys W, Marathe P, and Lai Y (2017) Physiologically based pharmacokinetic modeling of transporter-mediated hepatic clearance and liver partitioning of oatp and oct substrates in cynomolgus monkeys. *AAPS J* **19:**1878-1889.

Musther H, Harwood MD, Yang J, Turner DB, Rostami-Hodjegan A, and Jamei M (2017) The Constraints, Construction, and Verification of a Strain-Specific Physiologically Based Pharmacokinetic Rat Model. *J Pharm Sci* **106:**2826-2838.

Naritomi Y, Terashita S, Kimura S, Suzuki A, Kagayama A, and Sugiyama Y (2001) Prediction of human hepatic clearance from in vivo animal experiments and in vitro metabolic studies with liver microsomes from animals and humans. *Drug Metab Dispos* **29:**1316-1324.

Oliver RE (1995) Development of a whole-body physiological model based on dispersion concepts to describe the pharmacokinetics of drug in the body, in: *Department of Pharmacy*, pp 246, University of Manchester, Manchester, UK.

Downloaded from dmd.aspetjournals.org at ASPET Journals on April 19, 2024

DMD Fast Forward. Published on October 4, 2022 as DOI: 10.1124/dmd.122.000994
This article has not been copyedited and formatted. The final version may differ from this version.

Oliver RE, Jones AF, and Rowland M (2001) A whole-body physiologically based pharmacokinetic model incorporating dispersion concepts: short and long time characteristics. *J Pharmacokinet Pharmacodyn* **28:**27-55.

Pang KS, Han YR, Noh K, Lee PI, and Rowland M (2019) Hepatic clearance concepts and misconceptions: Why the well-stirred model is still used even though it is not physiologic reality? *Biochem Pharmacol* **169:**113596.

Pang KS and Rowland M (1977) Hepatic clearance of drugs. I. Theoretical considerations of a "well-stirred" model and a "parallel tube" model. Influence of hepatic blood flow, plasma and blood cell binding, and the hepatocellular enzymatic activity on hepatic drug clearance. *J Pharmacokinet Biopharm* **5:**625-653.

Plowchalk DR, Andersen ME, and deBethizy JD (1992) A physiologically based pharmacokinetic model for nicotine disposition in the Sprague-Dawley rat. *Toxicol Appl Pharmacol* **116:**177-188.

Poulin P and Theil FP (2002a) Prediction of pharmacokinetics prior to in vivo studies. 1. Mechanism-based prediction of volume of distribution. *J Pharm Sci* **91:**129-156.

Poulin P and Theil FP (2002b) Prediction of pharmacokinetics prior to in vivo studies. II. Generic physiologically based pharmacokinetic models of drug disposition. *J Pharm Sci* **91:**1358-1370.

Rane A, Wilkinson GR, and Shand DG (1977) Prediction of hepatic extraction ratio from in vitro measurement of intrinsic clearance. *J Pharmacol Exp Ther* **200:**420-424.

Roberts MS and Rowland M (1986a) A dispersion model of hepatic elimination: 1. Formulation of the model and bolus considerations. *J Pharmacokinet Biopharm* **14:**227-260.

Roberts MS and Rowland M (1986b) A dispersion model of hepatic elimination: 2. Steady-state considerations--influence of hepatic blood flow, binding within blood, and hepatocellular enzyme activity. *J Pharmacokinet Biopharm* **14:**261-288.

Rodgers T and Rowland M (2006) Physiologically based pharmacokinetic modelling 2: predicting the tissue distribution of acids, very weak bases, neutrals and zwitterions. *J Pharm Sci* **95:**1238-1257.

Rowland M (1972) Influence of route of administration on drug availability. *J Pharm Sci* **61:**70-74.

Rowland M, Benet LZ, and Graham GG (1973) Clearance concepts in pharmacokinetics. *J Pharmacokinet Biopharm* **1:**123-136.

Rowland M and Pang KS (2018) Commentary on "The universally unrecognized assumption in predicting drug clearance and organ extraction ratio". *Clin Pharmacol Ther* **103:**386-388.

Rowland M, Roberts MS, and Pang KS (2022) In defense of current concepts and applications of clearance in drug development and therapeutics. *Drug Metab Dispos* **50:**187-190.

Schneck DW, Pritchard JF, and Hayes AH, Jr. (1977) Studies on the uptake and binding of propranolol by rat tissues. *J Pharmacol Exp Ther* **203:**621-629.

Shibasaki S, Asahina M, Kawamata Y, Kojo M, Nishigaki R, and Umemura K (1989) The inhibitory effects of cimetidine on elimination and distribution of propranolol in rats. *J Pharmacobiodyn* **12:**549-557.

Sirianni GL and Pang KS (1997) Organ clearance concepts: new perspectives on old principles. *J Pharmacokinet Biopharm* **25:**449-470.

Sodhi JK, Wang HJ, and Benet LZ (2020) Are there any experimental perfusion data that preferentially support the dispersion and parallel-tube models over the well-stirred model of organ elimination? *Drug Metab Dispos* **48:**537-543.

Song D, Sun L, DuBois DC, Almon RR, Meng S, and Jusko WJ (2020) Physiologically based pharmacokinetics of dexamethasone in rats. *Drug Metab Dispos* **48:**811-818.

Sugita O, Sawada Y, Sugiyama Y, Iga T, and Hanano M (1982) Physiologically based pharmacokinetics of drug-drug interaction: a study of tolbutamide-sulfonamide interaction in rats. *J Pharmacokinet Biopharm* **10:**297-316.

Downloaded from dmd.aspetjournals.org at ASPET Journals on April 19, 2024

DMD Fast Forward. Published on October 4, 2022 as DOI: 10.1124/dmd.122.000994
This article has not been copyedited and formatted. The final version may differ from this version.

Tietz PS, Yamazaki K, and LaRusso NF (1990) Time-dependent effects of chloroquine on pH of hepatocyte lysosomes. *Biochem Pharmacol* **40:**1419-1421.

Tirona RG and Pang KS (1996) Sequestered endoplasmic reticulum space for sequential metabolism of salicylamide. Coupling of hydroxylation and glucuronidation. *Drug Metab Dispos* **24:**821-833.

Vermeulen NP, Danhof M, Setiawan I, and Breimer DD (1983) Disposition of hexobarbital in the rat. Estimation of "first-pass" elimination and influence of ether anesthesia. *J Pharmacol Exp Ther* **226:**201-205.

Watanabe T, Kusuhara H, Maeda K, Shitara Y, and Sugiyama Y (2009) Physiologically based pharmacokinetic modeling to predict transporter-mediated clearance and distribution of pravastatin in humans. *J Pharmacol Exp Ther* **328:**652-662.

Wilkinson GR and Shand DG (1975) Commentary: a physiological approach to hepatic drug clearance. *Clin Pharmacol Ther* **18:**377-390.

Yamano K, Yamamoto K, Kotaki H, Takedomi S, Matsuo H, Sawada Y, and Iga T (2000) Quantitative prediction of metabolic inhibition of midazolam by erythromycin, diltiazem, and verapamil in rats: implication of concentrative uptake of inhibitors into liver. *J Pharmacol Exp Ther* **292:**1118-1126.

Zheng N, Zhang X, and Rosania GR (2011) Effect of phospholipidosis on the cellular pharmacokinetics of chloroquine. *J Pharmacol Exp Ther* **336:**661-671.

Downloaded from dmd.aspetjournals.org at ASPET Journals on April 19, 2024

DMD Fast Forward. Published on October 4, 2022 as DOI: 10.1124/dmd.122.000994
This article has not been copyedited and formatted. The final version may differ from this version.

Footnotes

This work was supported by NIH Grant R35 GM131800. No author has an actual or perceived conflict of interest with the contents of this article.

Downloaded from dmd.aspetjournals.org at ASPET Journals on April 19, 2024

DMD Fast Forward. Published on October 4, 2022 as DOI: 10.1124/dmd.122.000994
This article has not been copyedited and formatted. The final version may differ from this version.

Figure Legends

Figure 1. Signature profiles of (A) clearances (CL_h & CL_{int}) *vs* ER, and (B) partition coefficients *Kp vs ER* for the indicated hepatic clearance models. The dashed horizontal lines indicate Q_h = 60.82 mL/min/kg in (A) and K_p^{ss} =1 in (B).

Figure 2. Blood and liver concentration-time profiles of 14 model compounds. Measured concentrations in blood and liver are indicated by solid symbols in red and black. Black solid lines show the model fittings of the blood data and colored solid lines depict the model fittings of the liver data (WSM: purple, DM: orange, PTM: blue). The estimated $f_{ub}CL_{int}$ and K_p (B_{max} and K_d for CQ and QD) values are listed for each of the model compounds with the same color coding as those for the liver model fittings.

Figure 3. Blood and liver concentration versus time data for verapamil (VEM) with model fittings and predictions. Hepatic clearance model-dependent average unbound liver blood/tissue concentrations simulated according to Eq. 5, 11, and 24 are shown as dashed lines. Closed symbols are measured values, and solid lines depict fittings by hepatic clearance models with the same color coding as those used in Figure 2.

Figure 4. Comparisons of the predicted K_p by *in silico* methods (A-D), C&G method (E) and AR method (F) with the WSM-estimated K_p. The solid line indicates unity and the dashed lines indicate 2-fold ranges from unity. The black and red symbols in (A-D) represent *in silico* $K_{p,pred}$ and $K_{p,exp}$ for each of the compounds.

Figure 5. Comparisons of the predicted K_p^{ss} by hepatic clearance models, AR method, and C&G method (A), and *in silico* methods (B: $K_{p,exp}$; C: $K_{p,pred}$) with the reported *in vivo* K_p^{ss}. The dashed lines indicate 2-fold ranges from unity. The data are color-coded for each compound and are connected by lines for better visualization.

Downloaded from dmd.aspetjournals.org at ASPET Journals on April 19, 2024

DMD Fast Forward. Published on October 4, 2022 as DOI: 10.1124/dmd.122.000994
This article has not been copyedited and formatted. The final version may differ from this version.

Figure 6. Effects of changing K_p on predicting the liver concentration-time profiles of DLZ by the WSM. Black circles are measured liver concentrations and color-coded dashed lines indicate model simulations with $K_{p,WSM}$ (26.03, purple), ±2-fold $K_{p,WSM}$ (red), ±5-fold $K_{p,WSM}$ (green), the lowest (M1 $K_{p,exp}$ = 4.33, orange) and highest (M3 $K_{p,pred}$ = 14.82, pink) *in silico* K_p. In all cases, $f_{ub}CL_{int,WSM}$ was fixed to 397 mL/min/kg.

Downloaded from dmd.aspetjournals.org at ASPET Journals on April 19, 2024

Tables

Table 1. Literature-reported Q_h (mL/min/kg) and *in vivo* liver K_p^{ss} of 14 model compounds.

Compound	Q_h (mL/min/kg) [a]	Reported K_p^{ss} [b]	Reference
Chloroquine (CQ)	60.8	420 [c]	(Earle et al., 1948)
		241~1939 [d]	(Liu and Jusko, 2021)
Tolbutamide (TB)	58.9	0.30	(Sugita et al., 1982)
Cyclosporine A (CyA)	47.2	16. 6	(Bernareggi and Rowland, 1991)
Ethoxybenzamide (EB)	58.8	1.40	(Lin et al., 1982)
Fingolimod (FTY720)	47.2	31.4 [e]	(Meno-Tetang et al., 2006)
Nicotine (NIC)	82.1	7.00	(Plowchalk et al., 1992)
Pentazocine (PTZ)	50.1	0.47	(Fujio et al., 1983)
Hexobarbital (HB)	58.8	1.3 [f]	(Igari et al., 1982)
Phenytoin (DPH)	49.2	0.88 [f]	(Itoh et al., 1988)
Quinidine (QD)	58.8	5.5~21.4 [d]	(Harashima et al., 1985)
Propranolol (PPN)	85.0	1.24 [f]	(Shibasaki et al., 1989)
Diazepam (DZP)	58.8	2.03 [f]	(Igari et al., 1983)

Downloaded from dmd.aspetjournals.org at ASPET Journals on April 19, 2024

DMD Fast Forward. Published on October 4, 2022 as DOI: 10.1124/dmd.122.000994
This article has not been copyedited and formatted. The final version may differ from this version.

Verapamil (VEM)	NA	10.1	(Yamano et al., 2000)
Diltiazem (DLZ)	NA	3.97	(Yamano et al., 2000)

[a] The Q_h values based on a 250-g rat applied in commercial software are 47.2 mL/min/kg in GastroPlus, 51.7 mL/min/kg in PK-Sim Version 9.1 (http://open-systemspharmacology.org), and 77.4 mL/min/kg in Simcyp (Certara UK Ltd., Simcyp Division, Sheffield, UK; Version 20.1) (Musther et al., 2017).

[b] The reported K_p^{ss} are the ratio of measured liver and plasma concentration at SS unless otherwise indicated.

[c] The single K_p^{ss} value of CQ is based on the C_p of 157 ng/mL achieved after daily administration of 25 mg CQ to rats for 10 days.

[d] The K_p^{ss} ranges of CQ and QD were obtained from the reported liver B_{max} and K_d in the source literature according to Eq. 5, 7, 25, 37, and 42 with the C_p range of 5~200 ng/mL for CQ and 0.7~5 μg/mL for QD that covers the plasma concentrations in the datasets.

[e] The K_p^{ss} of FTY720 was calculated from the reported PBPK model-estimated K_p according to Eq. 42.

[f] The K_p^{ss} of HB, DZP, DPH and PPN were obtained from the reported $K_{p,C\&G}$ using Eq. 46.

NA: not available

Downloaded from dmd.aspetjournals.org at ASPET Journals on April 19, 2024

DMD Fast Forward. Published on October 4, 2022 as DOI: 10.1124/dmd.122.000994
This article has not been copyedited and formatted. The final version may differ from this version.

Table 2. Estimation of CL_b (mL/min/kg), ER, and $f_{ub}CL_{int}$ (mL/min/kg) from the blood PK data in rats for the model compounds.

Compound [a]	ER [b]		CL_b or CL_h [b]		$f_{ub}CL_{int}$ (CV%) [c]		
	Estimated (CV%)	Reported /Calculated	Estimated (CV%) [d]	Reported /Calculated	WSM	DM	PTM
TB	0.032 (3.3)	0.03	1.86	1.41	1.99 (3.3)	1.98	1.96 (3.3)
CQ [e]	0.033 (7.6)	0.195	2.01	11.5	2.08 (7.8)	2.06	2.04 (7.7)
CyA	0.06 (1.6)	0.08	2.77	3.7	3.79 (1.7)	3.75	3.68 (1.7)
EB	0.08 (6.3)	0.12	4.92	7.11	5.55 (4.9)	5.45	5.31 (4.7)
FTY720	0.17 (7.05)	0.18	7.89	8.28	12.2 (8.5)	11.8	11.1 (7.7)
NIC	0.39 (3.1)	0.55	29.49	45	38.2 (5.1)	34.3	29.6 (4)
PTZ	0.41 (1.9)	0.82	20.55	41.3	42.2 (3.2)	37.6	32.1 (2.5)
HB	0.46 (2.7)	0.64	27.33	37.6	52.8 (5)	45.8	38 (3.7)
DPH	0.55 (2.1)	0.61	26.93	30.1	73.6 (4.7)	61	48.2 (3.2)
QD [e]	0.58 (2.1)	0.85	34.2	49.7	84.5 (5)	69.5	53 (3.3)
PPN	0.59 (3.5)	0.77	49.9	65.7	86.4 (8.5)	69.7	53.8 (5.7)
DZP	0.66 (5.7)	0.65	38.8	38.22	118 (16.9)	89.8	65.6 (10.3)

Downloaded from dmd.aspetjournals.org at ASPET Journals on April 19, 2024

DMD Fast Forward. Published on October 4, 2022 as DOI: 10.1124/dmd.122.000994
This article has not been copyedited and formatted. The final version may differ from this version.

VEM	0.7 (1.4)	0.75	42.8	45.7	145 (4.6)	105	74.1 (2.7)
DLZ	0.87 (2.1)	0.85	52.7	51.7	397 (15.7)	213	123 (6.7)

[a] Literature sources for the modeling datasets, and the reported/calculated CL_b and ER were the same as those in Table 1 except for the following: the modeling datasets of CQ, CyA, EB, and PPN were obtained from (Adelusi and Salako, 1982), (Kawai et al., 1998), (Lin et al., 1978), and (Schneck et al., 1977); the reported/calculated ER of HB, DZP, and DLZ were obtained from (Vermeulen et al., 1983), (Igari et al., 1984), and (Naritomi et al., 2001).

[b] If ER was directly available from the literature, CL_b was calculated from Q_hER using the reported Q_h in Table 1 except for VEM for which the Q_h value of 60.82 mL/min/kg (Brown et al., 1997) was used since the reported Q_h was not available from the source literature (Yamano et al., 2000); otherwise, if only the CL_b was reported, ER was obtained from CL_b/Q_h. CL_b was assumed to be equal to CL_h for all compounds except for CQ and NIC for which the CL_h were obtained by subtracting their known extrahepatic CL from CL_b (Plowchalk et al., 1992; Liu and Jusko, 2021).

[c] With the estimated ER, $f_{ub}CL_{int}$ for the WSM, PTM, and DM were calculated using the Q_h of 60.82 mL/min/kg (Brown et al., 1997) according to Eq. 9, 16, and 28; the simulated R_N (Figure S1) were used for the calculation of $f_{ub}CL_{int}$ for the DM.

[d] CL_b have the same CV% values as those of estimated ER.

[e] The reported/calculated ER of CQ was calculated from the reported Q_h and $f_{ub}CL_{int}$ (Liu and Jusko, 2021) using Eq. 8, and the calculated CL_b was obtained from Q_hER. For QD, the reported CL_b was calculated from the reported plasma clearance (Harashima et al., 1985) by dividing R_b and the reported ER was obtained from CL_b/Q_h.

Downloaded from dmd.aspetjournals.org at ASPET Journals on April 19, 2024

DMD Fast Forward. Published on October 4, 2022 as DOI: 10.1124/dmd.122.000994
This article has not been copyedited and formatted. The final version may differ from this version.

Table 3. Summary of *in vivo* liver K_p and K_p^{ss} values for the model compounds as obtained by the hepatic clearance models, Area Ratio (AR), and Chen and Gross (C&G) methods.

Compound	ER [a]	Hepatic model estimated K_p (CV%)			$K_{p,\ C\&G}$	$K_{p,\ AR}$	Estimated K_p^{ss} [b]	
		$K_{p,\ WSM}$	$K_{p,\ DM}$	$K_{p,\ PTM}$			Hepatic models	C&G Method
TB	0.032	0.162 (7.8)	0.161 (7.8)	0.159 (7.8)	0.162	0.28	0.157	0.156
CQ [c]	0.033	B_{max}=12 (12.8) K_d=0.008 (27.7)	B_{max}=12 (12.9) K_d=0.008 (27.7)	B_{max}=12 (12.9) K_d=0.0081 (27.7)	175.6	169.7	55~470	170.3
CyA	0.06	14.3 (24.7)	14.2 (24.7)	13.9 (24.7)	9.52	13.5	13.5	8.95
EB	0.08	1.15 (20.7)	1.13 (20.6)	1.1 (20.7)	1.43	1.05	1.05	1.32
FTY720	0.17	50.46 (9)	48.67 (9)	46.02 (9)	57.51	41.83	42.02	47.74
NIC	0.39	9.86 (14.3)	8.86 (14.3)	7.65 (14.3)	7.78	6.35	6.06	4.75
PTZ	0.41	0.5 (9.7)	0.48 (9.8)	0.37 (9.7)	0.54	0.36	0.30	0.32
HB	0.46	2.04 (21.8)	1.65 (21.3)	1.46 (21.8)	2.29	1.09	1.09	1.07
DPH	0.55	2.85 (23.4)	2.36 (23.4)	1.87 (23.4)	2.94	1.29	1.29	1.32

Downloaded from dmd.aspetjournals.org at ASPET Journals on April 19, 2024

DMD Fast Forward. Published on October 4, 2022 as DOI: 10.1124/dmd.122.000994
This article has not been copyedited and formatted. The final version may differ from this version.

QD [c]	0.58	B_{max}=34.15 (8.9) K_d=0.014 (126)	B_{max}=33.76 (8.9) K_d=0.017 (130)	B_{max}=33.8 (8.8) K_d=0.021 (135)	97.61	57.8	6.7~43	40.99
PPN	0.59	1.27 (35.2)	1.03 (35.2)	0.79 (35.2)	1.01	0.52	0.52	0.42
DZP	0.66	9.52 (19.1)	7.24 (19)	5.29 (19.1)	4.37	3.23	3.24	1.49
VEM	0.7	24.8 (4)	18 (4)	12.7 (4)	28.82	7.30	7.33	8.52
DLZ	0.87	26.03 (7)	13.96 (7)	8.05 (7)	30.81	3.45	3.46	4.09

[a] The estimated *ER* in Table 2 were listed.

[b] The K_p^{ss} were calculated using Eq.41 for the hepatic models and Eq. 46 for the C&G method except that the values for CQ and QD were simulated by Eq. 5, 7, 25, 37, and 42 with the C_p range of 5~200 ng/mL for CQ and 0.7~5 μg/mL for QD.

[c] The unit of B_{max} and K_d is μg/mL for both CQ and QD.

Downloaded from dmd.aspetjournals.org at ASPET Journals on April 19, 2024

DMD Fast Forward. Published on October 4, 2022 as DOI: 10.1124/dmd.122.000994
This article has not been copyedited and formatted. The final version may differ from this version.

Table 4. Prediction of liver K_p of the model compounds by several *in silico* methods incorporated in GastroPlus.

Compound	*ER*	*In silico* $K_{p,\ pred}$ [a]				*In silico* $K_{p,\ exp}$ [b]			
		M1	M2	M3	M4	M1	M2	M3	M4
TB	0.031	2.08	0.68	0.11	0.11	2.87	1.68	0.17	0.17
CQ	0.033	7.15	12.63	28.52	3579	9.01	12.88	152.7	357.55 [c]
CyA	0.06	5.60	3.75	4.64	4.64	4.28	1.31	1.16	1.16
EB	0.08	0.82	0.67	0.48	0.48	0.75	0.72	0.63	0.63
FTY720	0.17	7.25	8.82	13.13	12.94	6.69	10.49	9.2	9.2
NIC	0.39	0.80	0.78	26.75	25.10	0.96	0.92	6.42	4.91
PTZ	0.41	7.10	9.98	20.24	18.07	7.27	11.91	27	25.59
HB	0.46	1.31	0.86	0.59	0.59	2.01	1.68	1.45	1.45
DPH	0.55	0.99	0.51	0.14	0.14	3.05	1.67	1.4	1.4
QD	0.58	4.41	3.57	16.09	12.88	7.19	7.98	28.38	26.65
PPN	0.59	5.44	4.71	21.90	21.72	6.41	5.71	18.89	18.74

Downloaded from dmd.aspetjournals.org at ASPET Journals on April 19, 2024

DMD Fast Forward. Published on October 4, 2022 as DOI: 10.1124/dmd.122.000994
This article has not been copyedited and formatted. The final version may differ from this version.

DZP	0.66	4.03	1.54	1.37	1.37	4.13	1.88	1.79	1.79
VEM	0.7	7.12	10.97	7.49	7.27	6.8	9.02	8.26	7.79
DLZ	0.87	7.19	8.47	14.82	13.53	4.33	2.49	10.36	7.27

[a] *In silico* K_p predicted using the physicochemical properties in the ADMET Predictor™ (Simulations Plus, Inc.) listed in Table S2.

[b] *In silico* K_p predicted using the experimentally determined physicochemical properties listed in Table S2.

[c] The M4 K_p of CQ (357.55) was obtained using the extended Lukacova method that includes lysosomal trapping (Assmus et al., 2017).

Downloaded from dmd.aspetjournals.org at ASPET Journals on April 19, 2024

DMD Fast Forward. Published on October 4, 2022 as DOI: 10.1124/dmd.122.000994
This article has not been copyedited and formatted. The final version may differ from this version.

DMD Fast Forward. Published on October 4, 2022 as DOI: 10.1124/dmd.122.000994
This article has not been copyedited and formatted. The final version may differ from this version.

Downloaded from dmd.aspetjournals.org at ASPET Journals on April 19, 2024

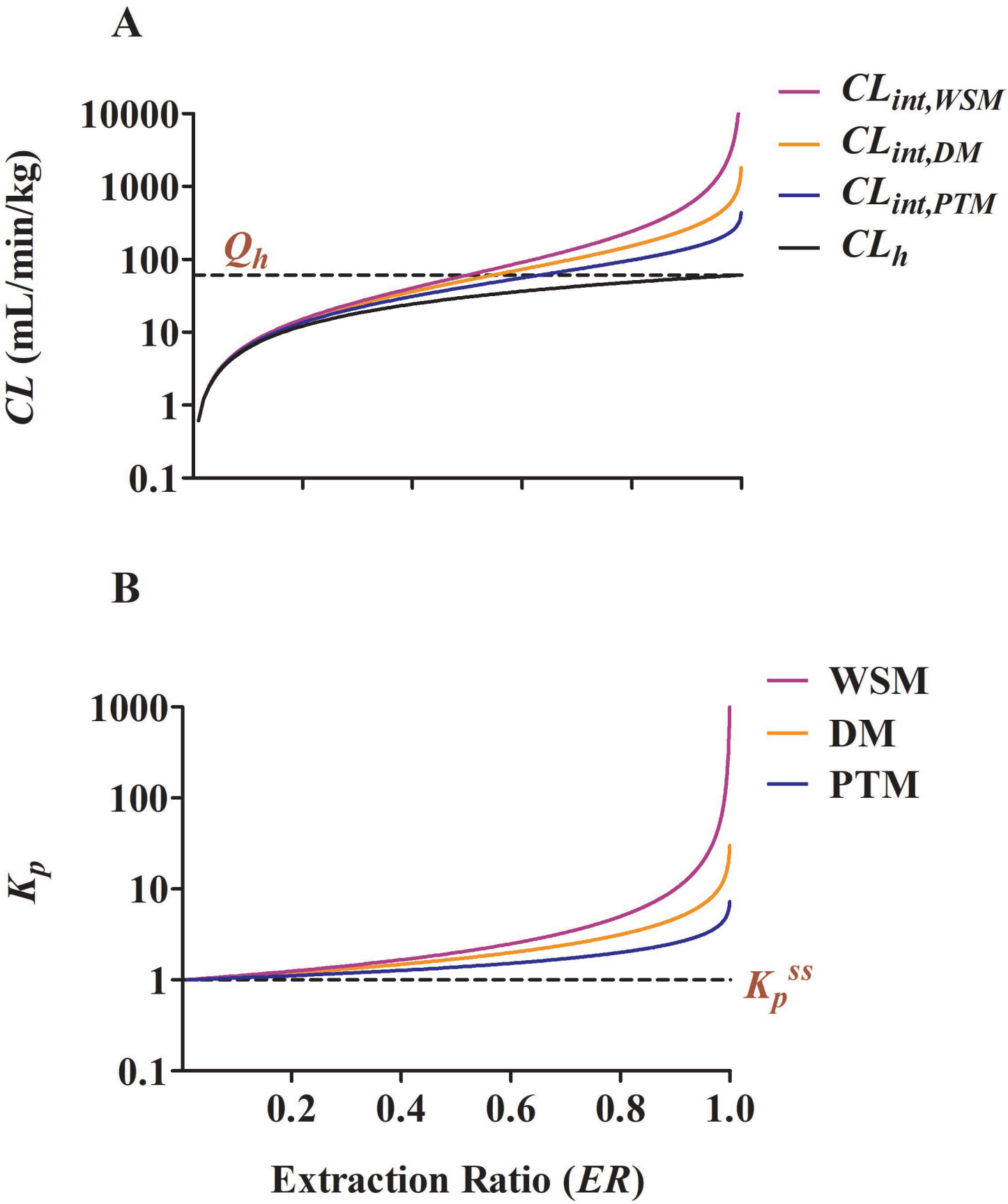
A
10000
1000
100
10
1
0.1
CL (mL/min/kg)
Qh
CLint,WSM
CLint,DM
CLint,PTM
CLh
B
1000
100
10
1
0.1
Kp
Kp ss
WSM
DM
PTM
0.2
0.4
0.6
0.8
1.0
Extraction Ratio (ER)

Fig. 1

This article has not been copyedited and formatted. The final version may differ from this version.

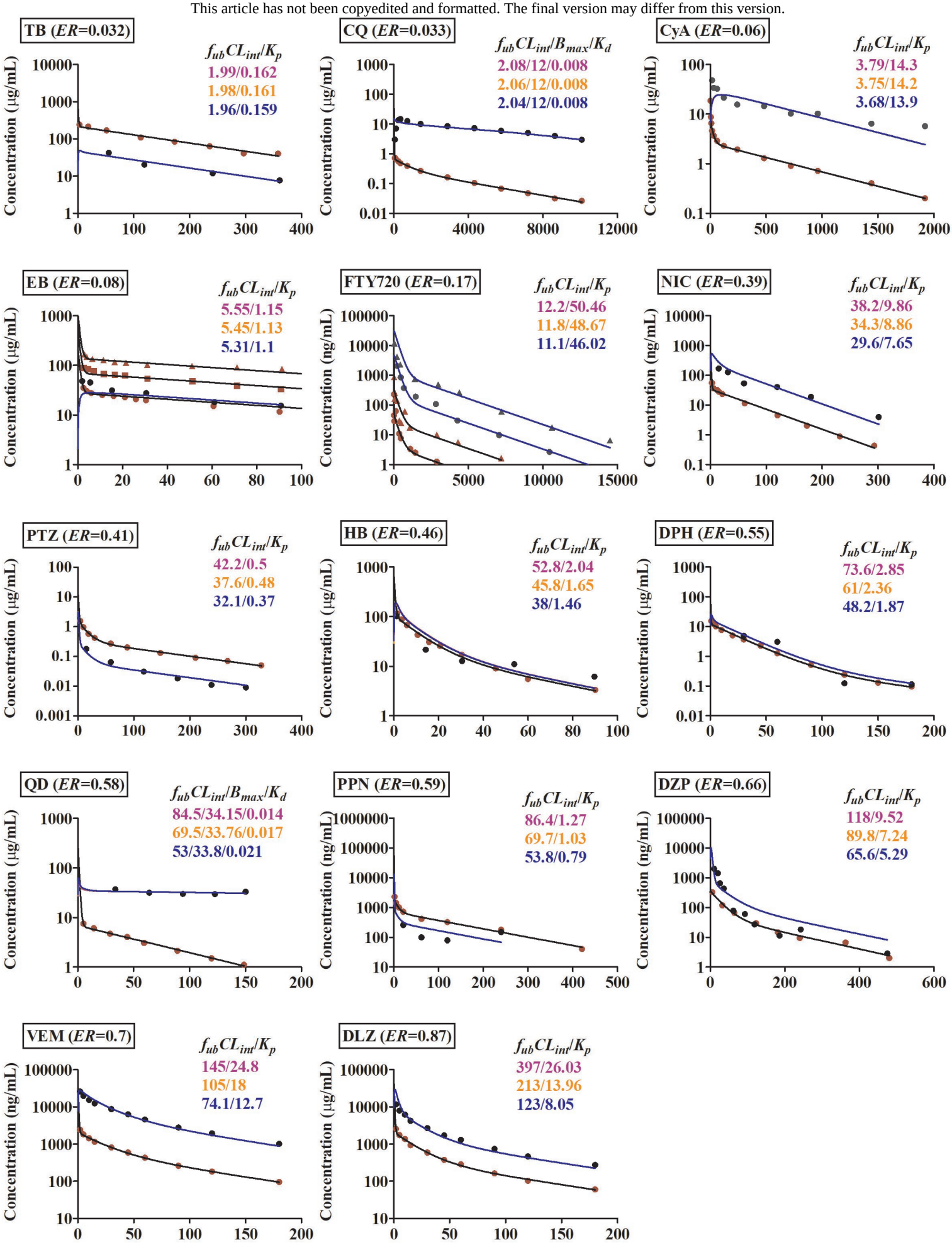

Fig. 2

Downloaded from dmd.aspetjournals.org at ASPET Journals on April 19, 2024

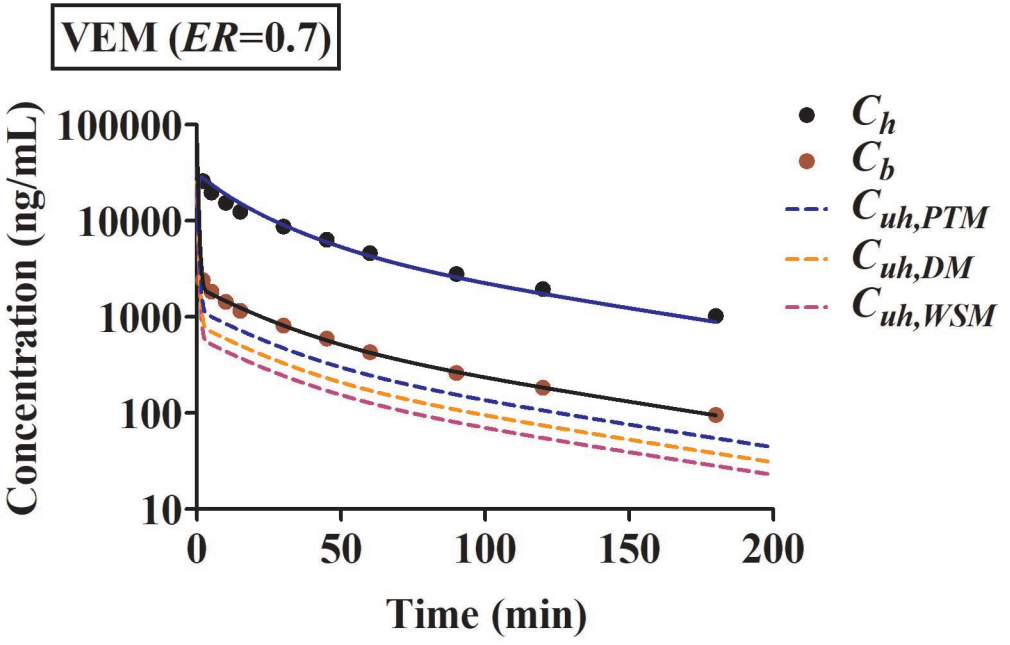
VEM (ER=0.7)
Concentration (ng/mL)
100000
10000
1000
100
10
0
50
100
150
200
Time (min)
C_h
C_b
$C_{uh,PTM}$
$C_{uh,DM}$
$C_{uh,WSM}$

Fig. 3

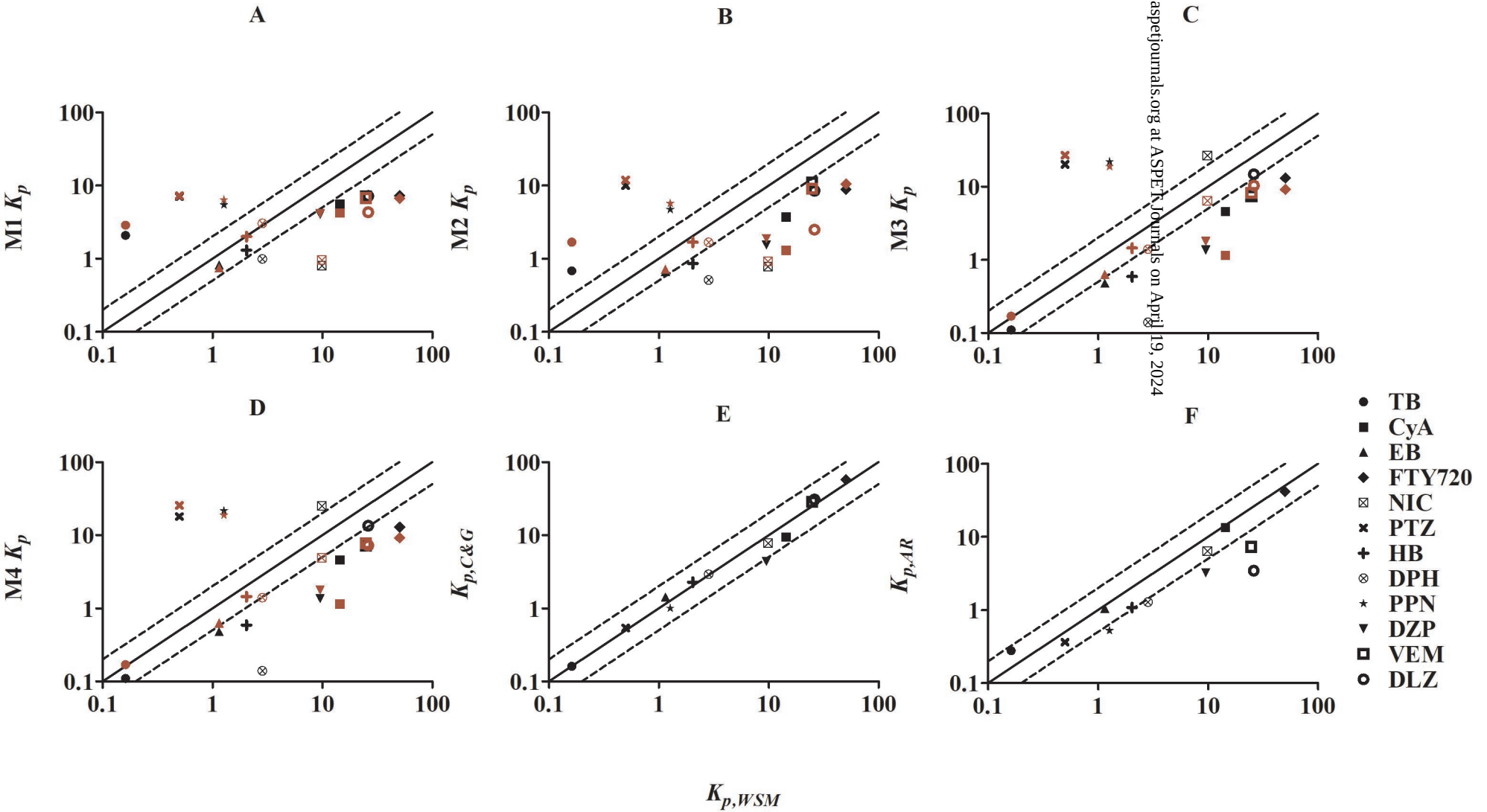

nd.aspetjournals.org at ASPET Journals on April 19, 2024

Fig. 4

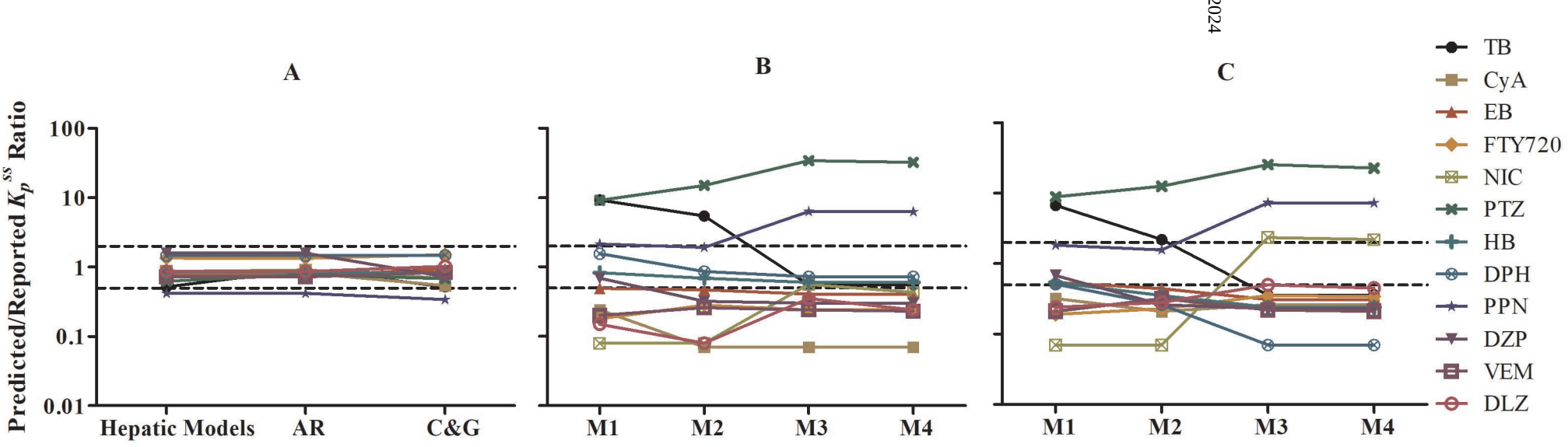
A
B
C
Predicted/Reported K_p^{ss} Ratio
100
10
1
0.1
0.01
Hepatic Models
AR
C&G
M1
M2
M3
M4
M1
M2
M3
M4
TB
CyA
EB
FTY720
NIC
PTZ
HB
DPH
PPN
DZP
VEM
DLZ

Fig. 5

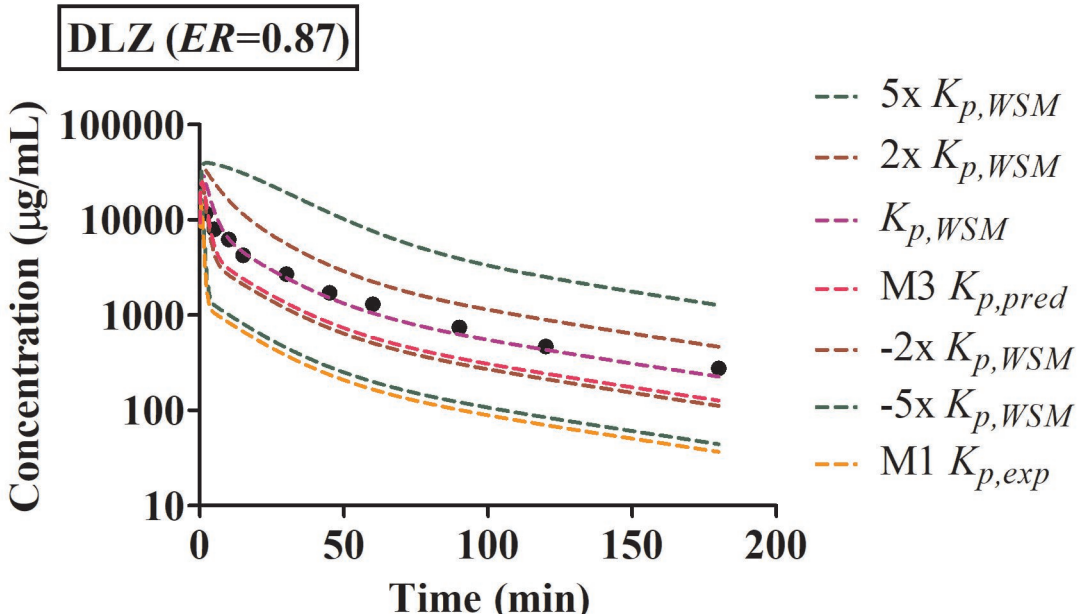
DLZ (ER=0.87)
Concentration (μg/mL)
100000
10000
1000
100
10
0
50
100
150
200
Time (min)
5x $K_{p,WSM}$
2x $K_{p,WSM}$
$K_{p,WSM}$
M3 $K_{p,pred}$
-2x $K_{p,WSM}$
-5x $K_{p,WSM}$
M1 $K_{p,exp}$

Fig. 6